Lab on a Chip

ROYAL SOCIETY OF CHEMISTRY

CRITICAL REVIEW

View Article Online
View Journal | View Issue

Cite this: *Lab Chip*, 2023, **23**, 1493

Recent progress of nanostructure-based enrichment of circulating tumor cells and downstream analysis

Lihua Guo,†[a] Chang Liu,†[a] Manlin Qi,[b] Liang Cheng,*[b] Lin Wang,[b] Chunxia Li*[c] and Biao Dong*[a]

The isolation and detection of circulating tumor cells (CTCs) play an important role in early cancer diagnosis and prognosis, providing easy access to identify metastatic cells before clinically detectable metastases. In the past 20 years, according to the heterogeneous expression of CTCs on the surface and their special physical properties (size, morphology, electricity, *etc.*), a series of *in vitro* enrichment methods of CTCs have been developed based on microfluidic chip technology, nanomaterials and various nanostructures. In recent years, the *in vivo* detection of CTCs has attracted considerable attention. Photoacoustic flow cytometry and fluorescence flow cytometry were used to detect CTCs in a noninvasive manner. In addition, flexible magnetic wire and indwelling intravascular non-circulating CTCs isolation system were developed for *in vivo* CTCs study. In the aspect of downstream analysis, gene analysis and drug sensitivity tests of enriched CTCs were developed based on various existing molecular analysis techniques. All of these studies constitute a complete study of CTCs. Although the existing reviews mainly focus on one aspect of capturing CTCs study, a review that includes the *in vivo* and *in vitro* capture and downstream analysis study of CTCs is highly needed. This review focuses on not only the classic work and latest research progress in *in vitro* capture but also includes the *in vivo* capture and downstream analysis, discussing the advantages and significance of the different research methods and providing new ideas for solving the heterogeneity and rarity of CTCs.

Received 24th September 2022,
Accepted 27th January 2023

DOI: 10.1039/d2lc00890d

rsc.li/loc

[a] *State Key Laboratory on Integrated Optoelectronics, College of Electronic Science and Engineering, Jilin University, Changchun, 130012, P. R. China. E-mail: dongb@jlu.edu.cn*
[b] *Department of Oral Implantology, Jilin Provincial Key Laboratory of Tooth Development and Bone Remodeling, School of Stomatology, Jilin University, Changchun, 130021, P. R. China. E-mail: chengliang@jlu.edu.cn*
[c] *Institute of Molecular Sciences and Engineering, Shandong University, Qingdao, 266237, P. R. China. E-mail: cxli@sdu.edu.cn*
† Theses authors contributed equally to this work.

1 Introduction

Cancer-related diseases are currently a major global health problem with approximately eight million deaths each year.[1] It is estimated that 28.4 million new cancer cases will occur in 2040, an increase of 47 percent over the corresponding 19.3 million cases in 2020.[2] Pathological analysis based on tumor tissue is the "gold standard" for cancer diagnosis. It

Lihua Guo

Ms. Lihua Guo received her Bachelor's degree from Jilin University, and is pursuing her Master's degree in Prof. Biao Dong's group at Jilin University. Her research focuses on nanomaterials-based circulating tumor cell enrichment.

Chang Liu

Mr. Chang Liu received his Bachelor's degree from Jilin University. Currently, he is a Master's student in Prof. Jianlong Yang's group in Shanghai Jiao Tong University. His research focuses on CTCs analysis and computational imaging.

relies on invasive methods, including surgical resection and needle aspiration. These tissues contain key information, including histopathology and molecular atlas, which helps to classify, diagnose and predict the progression of cancer. However, invasive sampling methods have certain limitations. First, invasive sampling is expensive and the procedure is complicated. Second, invasive sampling methods may put patients at risk of injury. For example, advanced prostate cancer metastases are often found in hardened bones and require a larger drill to sample. In addition, tumors are recognized as having spatio-temporal heterogeneity, that is, the extent to which the biopsy sample can represent the tumor itself biologically and molecularly, depending on the sampling location and will change with the passage of treatment time. If the occurrence and metastasis of tumors can be detected earlier through non-invasive methods, the suffering of patients can be greatly reduced, tumors may be treated at an early stage, and the treatment and prognosis of cancer can be improved.

Circulating tumor cells (CTCs) are cancer cells that shed from a primary tumor and spread to other organs through the bloodstream.[3] CTCs may play a key role in cancer metastasis and is responsible for more than 90% of cancer-related deaths.[4,5] CTCs are considered to contain the same genetic information with the CTCs of the primary tumor and metastatic sites. Therefore, a better understanding of CTCs is beneficial for exploring the mechanisms of primary tumor and metastasis. Isolation of these CTCs from blood, commonly referred to as a "liquid biopsy," provides a minimally invasive method to obtain cancer cells for enumeration or molecular and cellular analysis.[6,7] The number of CTCs has been shown to be predictive of cancer prognosis and may also assist with characterizing treatment efficacy.[8] Indeed, an increase in CTCs may indicate that chemotherapy is no longer effective or that the cancer has changed, making tumor cells more resistant to current treatments.[9] In particular, the number of CTCs can be used as an independent predictor and prognostic marker for various cancers, such as breast, prostate, liver, colorectal, and ovarian cancers.[10–13] Molecular profiling of CTCs, such as monitoring of heterogeneous phenotypes, resistance from gene mutations, and functional protein activity, may provide insights into the mechanisms of cancer progression, and guide diagnosis and precise personalized therapy.[14–19] Despite the enormous clinical value mentioned above, CTC analysis has not yet entered routine clinical practice. This is mainly due to the lack of practical techniques to isolate these rare, highly sensitive and selective tumor cells. Due to the difficulty of obtaining CTCs, understanding the mechanism of tumor metastasis through CTC analysis remains a great challenge.

CTCs carry a large amount of information about tumor occurrence, development, metastasis and drug resistance, and can provide real-time information about patient staging (metastatic and non-metastatic) and tumor molecular characteristics. The detection and diagnosis of CTCs provide extensive diagnosis and support for the early diagnosis of cancer metastasis, and might provide the entire development process of CTCs. From the earliest *in vitro* detection of blood collection based on the physical properties of CTCs, a lot of novel platforms and technologies have been developed for CTCs detection in the last two decades (Fig. 1). The method of *in vitro* testing refers to two processes, including extraction of blood from patients, as well as CTCs isolation from the whole blood. At present, the *in vitro* separation of CTCs is mostly based on microfluidic technology, which is captured according to the physical characteristics (size, density, dielectric properties, *etc.*) and biological characteristics of

Chunxia Li

Prof. Chunxia Li is a Professor at Shandong University, and received her Ph.D. degree (2008) from the Changchun Institute of Applied Chemistry, Chinese Academy of Sciences under the guidance of Prof. Jun Lin. After graduation, she became an Assistant Professor in Prof. Lin's group and was promoted to Associate Professor in 2012. Then, she worked as a Professor at Zhejiang Normal University from 2016 to 2019. Her current research interests include the controllable synthesis of multifunctional nanomaterials and their bioapplications.

Biao Dong

Prof. Biao Dong is a Professor of State Key Laboratory on Integrated Optoelectronics, College of Electronic Science and Engineering, Jilin University. He obtained his Ph.D. degree in 2008 from the Chinese Academy of Science. From 2012 to 2014, he worked as a Postdoctoral Fellow in Laboratoire Catalyse et Spectrochimie (LCS) de l'Université de Caen (France) under the supervision of Prof. Svetlana Mintova. He won the Gilles KAHN Prize in 2016 from FFCSA. He is currently the Director of the Department of Biomedical Engineering. His current research interests include the multifunctional nanomaterials design, and their bioapplications in tumor and periodontal disease therapy and detection

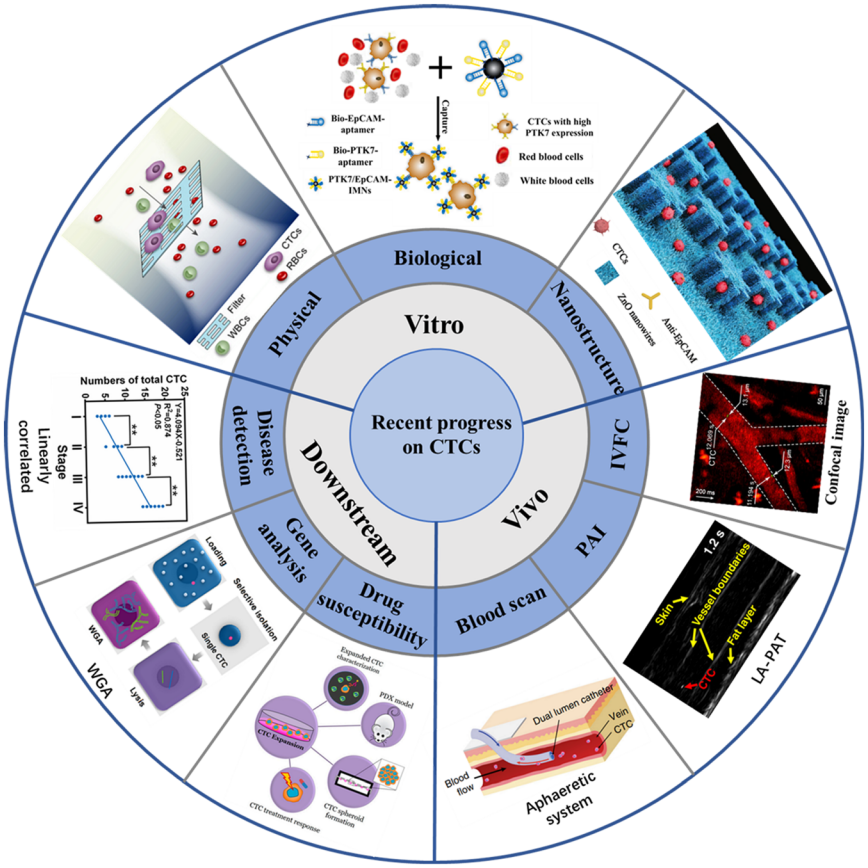

Fig. 1 Schematic illustration of the recent progress of CTCs on enrichment *in vitro*, enrichment *in vivo*, and downstream analysis[20–28] (reproduced with permission from ref. 20, Copyright 2022, Royal Society of Chemistry; reproduced with permission from ref. 21, Copyright 2022, American Chemical Society; reproduced with permission from ref. 22, Copyright 2020, Royal Society of Chemistry; reproduced with permission from ref. 23, Copyright 2018, John Wiley and Sons; reproduced with permission from ref. 24, Copyright 2018, SPIE; reproduced with permission from ref. 25, Copyright 2019, Springer Nature; reproduced with permission from ref. 26, Copyright 2020, MDPI; reproduced with permission from ref. 27, Copyright 2022, American Chemical Society; reproduced with permission from ref. 28, Copyright 2022, American Chemical Society).

CTCs. In addition, there is a nanoscale interaction between nanostructures and CTCs, which is conducive to cell capture and culture. In recent years, there have been many enrichment methods of CTCs based on nanomaterials or nano-surfaces, such as using antibody-modified magnetic beads and cleverly designed antibodies to modify the microstructure. Compared with conventional invasive biopsy, *in vitro* test samples are easy to sample, and have the advantages of high specificity and good patient compliance. *In vivo* detection refers to implanting a designed capture platform into the body or injecting molecules for imaging into a patient's vein, and directly detecting CTCs in the blood in the patient's normal physiological environment. One example is inserting the retention needle of the antibody-modified outer wall into the venous blood vessel, which can stay in the blood for a long time. CTCs can be efficiently captured when a large amount of blood is flowing through it. There are also studies using photoacoustic imaging technology to directly observe CTCs in venous blood vessels. In some technologies, the cells captured and fixed in the vein can be killed *in situ* in the body by photothermal effect, which has important clinical significance for adjuvant cancer treatment and provides new ideas for the prevention of tumor metastasis. The advantage of *in vivo* testing is that the target blood volume is large (whole body blood ~5 L), CTCs can be detected under normal physiological environment, and possible contamination during the sampling processing is avoided. At the same time, it can detect CTCs from various parts of the body, so that subsequent molecular level analysis can provide more comprehensive information. Because CTCs can provide real-time, comprehensive and accurate tumor biological information, it also has a lot of room for development in clinical application. At present, the downstream analytical applications of CTCs include prognosis assessment, adjuvant targeted therapy, and drug sensitivity testing.

In this review, we introduce various recently developed CTC enrichment technologies that are categorized based on physical and biological characteristics, summarize various emerging detection technologies based on nanostructures, and provide detailed information about the latest CTC-based technologies and clinical applications. This article may be a useful guide for cancer research scientists and oncologists to understand various CTCs detection methods and

downstream analysis techniques. A better understanding of CTC-based technologies and anticipated future developments promises to improve the treatment and diagnosis of cancer patients.

2 Technologies for CTC enrichment *in vitro*

2.1 Physical properties for isolation

After tumor cells enter the circulatory system, metabolic abnormalities and metabolic disorders, cell composition, gene expression and modification, as well as the protein synthesis and polymerization of certain polar particulate matter change. This causes the physical properties of CTCs entering the circulatory system to be different from other cells in the blood vessels, which makes it possible to separate CTCs from whole blood based on physical properties.

2.1.1 Size and morphology. In general, the average diameter of white blood cells (WBC) is 7–20 μm; the diameter of red blood cells (RBC) is 6–9 μm; and the diameter of a platelet is 2–4 μm.[29] The average diameter of cancer cell lines used to verify various CTCs separation techniques is 15–25 μm (there is also a literature study saying 9–19 μm),[30,31] which is larger than WBC and other cells in blood vessels. The main advantage of size-based separation technology is that it can quickly and easily capture unlabeled, unmodified living cells for subsequent downstream analysis. Moreover, because it does not require expensive biochemical label modification, size-based technology has a shorter enrichment time and lower expected cost.

Membrane microfilters and microfluidic devices are the most commonly used size-based CTCs separation technologies. According to the difference in size and deformability of tumor cells and blood cells, Hosokawa *et al.* designed a microfluidic device equipped with size-selective microcavity array for the efficient and rapid detection of tumor cells in blood.[32] The device allows for detection of breast, stomach and colon tumor cell lines, including EpCAM-negative tumor cells, which cannot be separated by conventional immunomagnetic separation, but have more than 80% capture efficiency in microcavity arrays. Zheng *et al.* made a size-based filtration device for CTCs detection by using parylene-C, which can complete cell analysis in 10 minutes, and the recovery rate of CTCs is 90%.[33] Based on the difference of size and deformation, Xu *et al.* separated CTCs from blood by microfilter, and used a Surface-

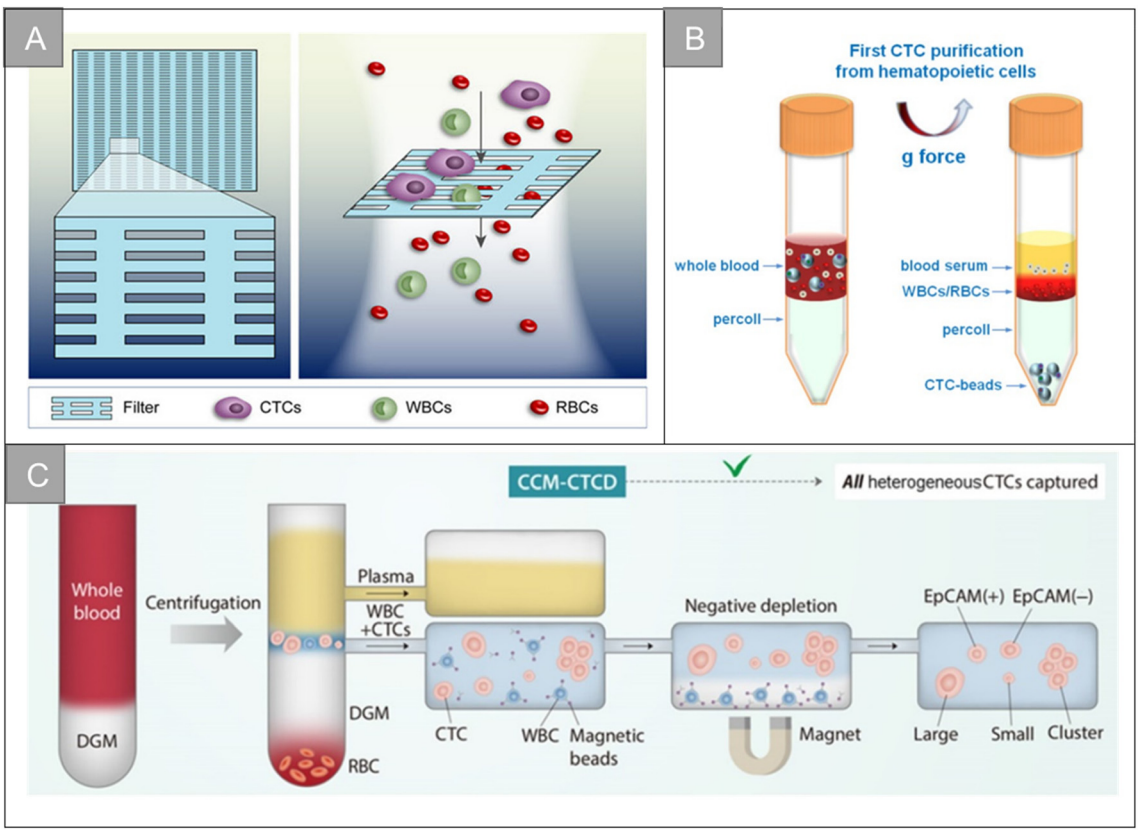

Fig. 2 Physical properties for isolation | (A) schematic diagram of the filtering mechanism of slit-shaped pores for efficient enrichment of CTCs[20] (reproduced with permission from ref. 20, Copyright 2022, Royal Society of Chemistry). (B) Schematic diagram of the centrifugation of live CTCs from hematopoietic cells by selective sedimentation with an improved centrifugation medium (Percoll) and CTC-beads[38] (reproduced with permission from ref. 38, Copyright 2018, Ivyspring International Publisher (**https://ivyspring.com/**)). (C) Schematic diagram of the CCM-CTCD extraction strategy resulting in the capture of all polyphyletic CTCs[39] (reproduced with permission from ref. 39, Copyright 2022, Ivyspring International Publisher (**https://ivyspring.com/**)).

Enhanced Raman Scattering (SERS) biological probe on the microfilter to realize the *in situ* isolating and direct detection of CTCs in peripheral blood.[34] As shown in Fig. 2A, Li *et al.* designed an ultra-thin Si_3N_4 filter membrane with slit pores, which is prepared by standard microfabrication process and easy for large-scale production, and successfully achieved efficient separation of CTCs from whole blood.[20] The pore diameter of the filter membrane is 6 nm, the thickness is 200 nm, and the porosity is as high as 34%. In the capture experiments of A549 cells and Hct-116 cells, the Si_3N_4 filter membrane showed high capture rate (96%), high leukocyte removal rate (99.99%) and high cell viability (90%). In the detection of clinical samples, the microfluidic chip can isolate CTCs from blood samples of cancer patients (5 patients with non-small cell lung cancer and 5 patients with colorectal cancer) and analyze the mutation of the EGFR gene, showing a good potential for clinical application.

Circulating tumor microemboli (or CTC cluster) accounts for about 2–5% of all CTCs, and is a cluster formed by multiple CTCs or CTC and other blood components. Compared with a single CTC, the CTC cluster is more hidden, can survive longer in peripheral blood, and has stronger invasive ability. A. Fatih Sarioglu *et al.* designed a size-based microfluidic chip for capturing CTC clusters in unprocessed blood.[35] The basic construction module of the chip is formed by three triangular columns, two of which form a narrowing channel that gathers cells into the opening, and the edge of the third column is positioned to bifurcate the laminar flow. With the blood flow, a single blood cell and a single CTCs flow into one of the two streamline lines, and the CTC clusters stay at the front of the bifurcation column under dynamic force balance. Mert Boya *et al.* designed the Cluster-Wells chip by combining the speed and practicability of membrane filtration with the sensitive and deterministic screening provided by the microfluidic chip.[36] Cluster-Wells chips capture CTC clusters in micropores, and individual cells in the blood will pass through the micropores. Once the CTC cluster enters the hole, it is confined to the grid by a sloping sidewall, and the 2 μm wide grid line ensures that the cell cluster enters different openings; the cell flow rate of 65 μm s^{-1} (about 10 times lower than the physiological free flow velocity in human capillaries) can prevent the cell cluster from dissociating. The number of micropores of the Cluster-Wells chip is more than 100 000. The micropores are uniformly distributed on the membrane with a diameter of 47 mm, which realizes the mild treatment of CTC clusters, while providing a processing rate of 25 mL h^{-1}, which can meet the clinical requirements and allow the recovery of viable clusters from the device.

2.1.2 Density. Density gradient centrifugation can separate cell types according to cell density, which is an important method for CTC enrichment. Ada Lee *et al.* designed an unlabeled CTCs separation platform based on centrifugal force, which can separate and count high purity CTCs from whole blood within 30 seconds.[37] Huang *et al.* developed a multifunctional density gradient centrifugation method based on microspheres to achieve effective CTC capture, as shown in Fig. 2B.[38] This method has been successfully used for high purity separation, mild release and downstream analysis of CTCs from patients with colorectal cancer and breast cancer. The release efficiency and survival rate of CTCs are 94% and 92.5%. In addition, the main experimental equipment of this method is standard centrifuge, which has high potential in clinical application. Hyeong Jung Woo *et al.* designed a fully automatic continuous centrifugal microfluidic system with high recovery and purity for a variety of CTCs populations, as shown in Fig. 2C (including EpCAM (+), EpCAM (−), small and large cancer cells and CTC clusters). The recovery rate is more than 90% and the depletion rate is 99.9%.[39] In addition, the detection and analysis of blood samples from 30 patients with non-small cell lung cancer showed that there was a good correlation between the EGFR mutation spectrum of CTCs and the spectrum of circulating tumor DNA (CtDNA). In patients with insufficient ctDNA for mutation analysis, CTC analysis may be an auxiliary decision-making tool.

2.1.3 Electrical properties. Dielectric electrophoresis (DEP), which is usually based on cell size and dielectric properties, is a real-time and controllable CTC capture method. At the same time, non-contact DEP can reduce cell damage and is beneficial to cell culture and downstream analysis. Cheng *et al.* designed a DEP-based V-shaped microfluidic platform for high-throughput separation of CTCs from diluted blood samples, as shown in Fig. 3A.[40] The chip has the characteristic of an adjustable channel length. When the sample passes through the long LDEP channel of 6 cm and the appropriate voltage with a frequency of 10 kHz at the optimal flow rate of 20 μL min^{-1}, about 85% of the cancer cell samples are recovered from 0.001%. Luo *et al.* combined unsheathed prefocusing and DEP separation based on gravity-sedimentation method. In a simple microfluidic device, cells are continuously separated according to their size or dielectric properties, and the separation efficiency can reach more than 90%.[41] Paresa Modarres *et al.* designed an adjustable microfluidic platform for particle separation based on the principle of frequency-hopping DEP.[42] In the proof-of-concept experiment of polystyrene particles, the separation efficiency is as high as 98.7%. In the experiment of diluted blood samples with MCF-7, the platform achieves a capture efficiency as high as 82.2%. Jongho Park *et al.* designed microfluidic devices based on microwell-on-electrode (MOE) to capture individual cells, and clustered cells simultaneously at the single cell/cluster level (Fig. 3B).[43] DEP is used to make cell-sized micropores on interdigitated electrodes to effectively capture a single cell or a cell composed of a cell cluster, with a high capture rate.

2.1.4 Acoustic properties. Acoustic electrophoresis is a robust, accurate and high-throughput method for unit operation of suspended cells. When exposed to standing acoustic waves, the cells suspended in the liquid are subjected to acoustic radiation force (ARF), and the cells are separated according to their sonophoresis mobility, resulting

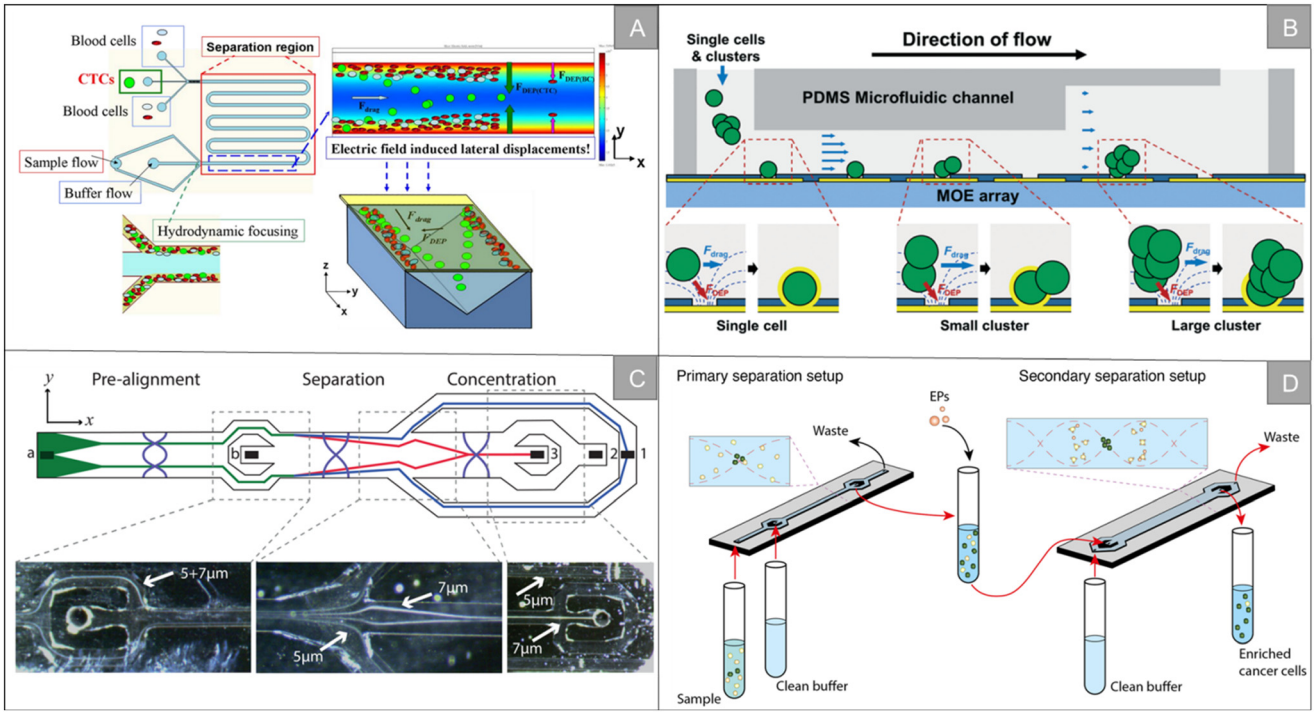

Fig. 3 Physical properties for isolation | (A) schematic diagram of the LDEP CTC isolation system[40] (reproduced with permission from ref. 40, Copyright 2015, Royal Society of Chemistry). (B) Schematic diagram of a microfluidic system for the simultaneous trapping of single and clustered cells by using a MOE device[43] (reproduced with permission from ref. 43, Copyright 2022, Royal Society of Chemistry). (C) Schematic illustration of the chip from the top showing particle trajectories and inset photographs, showing the separation of 5 and 7 μm polystyrene particles[45] (reproduced with permission from ref. 45, Copyright 2015, American Chemical Society). (D) Schematic illustration of the workflow and separation principle in A^2 (ref. 47) (reproduced with permission from ref. 47, Copyright 2021, published by American Chemical Society).

in specific lateral displacement of the cells when they flow through the channel. Per Augustsson *et al.* designed a non-contact and label-free microfluidic sonoelectrophoresis method, which separated prostate cancer cells (DU145, PC3, LNCaP) from WBC by the force generated by ultrasonic resonance in microfluidic channels.[44] Maria Antfolk *et al.* designed a microfluidic cell sorter based on acoustic electrophoresis, which realized the simultaneous separation and volume concentration of cells without labels, and the mild treatment method was convenient for subsequent analysis or cell culture (Fig. 3C).[45] The equipment uses ultrasonic standing wave to pre-align, separate, and concentrate cells and particles. The recovery rate of 7 μm polystyrene particles is 99.3 ± 0.3% and the contamination concentration is 0.1 ± 0.03%. At the flow rate of 100 μL min^{-1}, the isolation rate of MCF-7 cells, the contamination rate of WBC, the isolation rate of DU145 cells, and the contamination rate of WBC were 91.8 ± 1.0%, 0.6 ± 0.1%, 84.1 ± 2.1% and 0.2 ± 0.04%, respectively. S. Karthick *et al.* designed a label-free method based on acoustic impedance contrast, which was used to separate peripheral blood mononuclear cells (PBMCs) from CTCs by acoustic electrophoresis in microchannels.[46] The method uses high acoustic impedance liquid to match the acoustic impedance of cell suspension medium with that of PBMCs, so as to prevent the lateral movement of PBMCs caused by ARF. Compared with PBMCs, CTCs with different acoustic impedance are allowed to laterally transfer due to ARF, thus being separated from PBMCs. The method has a blood throughput of 2 mL h^{-1}, and the recovery rate of HeLa and MDA-MB-231 cells is >86% and >50-fold enrichment. Eva Undvall Anand *et al.* developed a two-step sequential sonophoresis (A^2) method, which was used to separate CTC from RBC lysed whole blood.[47] These two steps are based on the acoustic translocation of cells and particles (Fig. 3D). First, through the primary separation step, the viable cancer cells are enriched at the central outlet according to the acoustic characteristics of the cells. The secondary purification step involves the removal of the contaminated WBCs by negative selection acoustic contrast.

2.1.5 Fluid mechanics. According to the working principle, all kinds of reported CTC microfluidic sorting devices can be divided into active and passive types. The active sorting device (active microfluidic sorting device) uses external (electric, magnetic, acoustic and optical) fields to realize cell separation according to the difference of size, refractive index and dielectric properties. A passive microfluidic sorting device uses inherent fluid effects (inertia, viscoelasticity, hydrophobicity, *etc.*) and specially designed microstructures (deterministic lateral displacement, spiral microfluidic, *etc.*) to sort cells according to their size, shape or deformability.

Inertial focusing utilizes fluid inertial effects in shaped microchannels to align particles and cells at high flow rates. When randomly dispersed particles flow through a channel with a particle Reynolds number of 1 or greater, they experience two counteracting inertial lift forces. The combination of these forces causes particles to migrate to two to four dynamic equilibrium positions located between the channel centerline and the wall.[48] After focusing, by subsequently dividing the channel into multiple outlets, the focused cell scans are collected in a smaller volume and focused significantly in a size-dependent manner.[49] Majid Ebrahimi Warkiani *et al.* used soft lithography technology to manufacture a spiral microfluidic chip for high-throughput separation and recovery of CTCs in blood (Fig. 4A).[50] The chip makes use of the inertia and Dean resistance in the spiral microfluidic device to focus the larger CTCs and the smaller blood cells to different positions, and achieves a peak cell recovery rate of more than 85% of multiple cancer cell lines. Tian *et al.* developed an interfacial viscoelastic microfluidic system by using the competition between the inertial lift and interfacial elastic lift.[51] This system can directly separate tumor cells from whole blood by size selection, with a separation efficiency of 95.1% and a recovery rate of 77.5%. The survival rate of tumor cells after separation is about 100%. R. Guglielmi *et al.* designed a spiral microfluidic chip, which separated WBC by inertial force and centrifugal force in a curved channel, thus realizing label-free enrichment of CTCs.[52] Fang *et al.* designed a small centrifuge based on inertial microfluidics.[53] The centrifuge is composed of four parallel inertial spiral channels and a two-stage serpentine channel connected in series, which realizes the efficient washing and concentration of biological samples (Fig. 4B). It has the advantages of simple manufacturing, convenient operation and small floor space. Experiments show that 10–20 μm particles can be eluted from the original sample, and the concentration is increased. The recovery rate is more than 93%. In addition, the centrifuge has been successfully applied to various biochemical experiments, including extracting target cells from original samples, purifying target biological particles from micro/nano-particle background, changing the culture medium of cultured MCF-7 breast cancer cells, extracting A549 lung cancer cells from

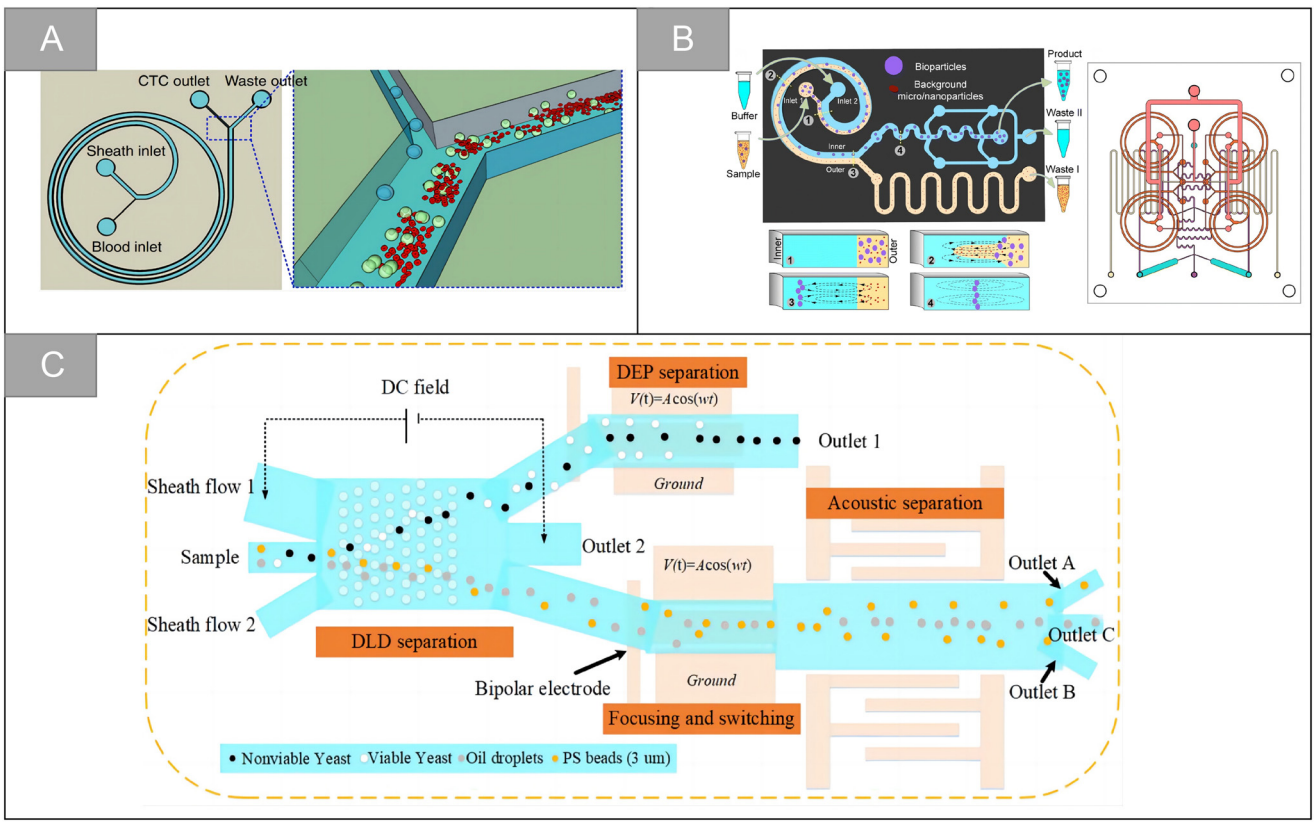

Fig. 4 Physical properties for isolation | (A) schematic diagram of CTCs isolation using spiral microfluidics[50] (reproduced with permission from ref. 50, Copyright 2015, Springer Nature). (B) Schematic diagram illustrating the working principle of miniaturized centrifuge and detailed structure of the integrated multilayer miniaturized centrifuge[53] (reproduced with permission from ref. 53, Copyright 2022, Royal Society of Chemistry). (C) Schematic illustration of the integrated microfluidic system designed to achieve multitarget separation[55] (reproduced with permission from ref. 55, Copyright 2021, American Chemical Society).

calcein-AM staining solution, purifying WBC from cracked whole blood, and extracting target cells from a background of unbound magnetic microbeads.

Although great success has been achieved, the microfluidic sorter using only a single technology still has the limitation of low capture purity. By integrating two or more different separation technologies, hybrid separation technology inherits the advantages of different technologies, which is beneficial to improve the separation performance and solve the limitations of a single technology. In recent years, it has attracted increasingly more attention. Xiang *et al.* combined inertial microfluidic with deterministic lateral displacement (DLD) to design a two-stage microfluidic sorting device.[54] A high-throughput spiral microfluidic channel is used as the first-stage sorter to remove most of the background cells to reduce the blocking risk of the next stage. The DLD sorting channel composed of triangular microcolumns is used in the second stage of sorting, so as to further remove the residual background cells and obtain high-purity target cells. The device improves the throughput and accuracy of cell sorting, the clearance rate of blood cells is 99.95%, and the average recovery rate of the tumor cells is 91.34%. Wu *et al.* designed a microfluidic chip with integrated sound field and electric field for multiple separation of mixed biological samples.[55] As shown in Fig. 4C, the chip consists of four modules: DLD array, bipolar electrode (BPE) focusing module, surface acoustic wave (SAW) sorting module and DEP sorting module. It has about 90% separation efficiency for selecting various types of cells and particles.

2.2 Biological properties for isolation

The separation technology based on biological characteristics is widely used among the existing CTC enrichment technologies. These technologies rely on the unique antigen expression of CTCs, related to their tissue origin and different from other normal components circulating in the blood, to identify CTCs precisely. EpCAM is the most commonly used target, expressed in epithelial cancers, and does not appear in normal cells of the circulatory system. However, CTC has a high degree of heterogeneity and epithelial–mesenchymal transition (EMT) process. Only using EpCAM as a target cannot enrich multiple subtypes of CTC. Therefore, new targets such as N-cadherin, CD44, HER2, and MUC1 are developed to enrich CTC. In addition to traditional antibodies, many CTC enrichment schemes based on aptamers, peptides, and chemical molecules have emerged in recent years. This section introduces CTC enrichment technology based on different targeting molecules.

2.2.1 Antibody. Immunomagnetic separation based on antibody-functionalized magnetic beads is the most widely used CTCs separation technology. At present, the gold standard is the CellSearch system in CTC field, which is the first technology approved by the FDA for clinical CTCs detection of prostate cancer, breast cancer and colorectal cancer, captures CTCs through this technology. However, the CellSearch system has limitations in purity, capture efficiency and sensitivity, which leaves room for improvement for the development of other cell capture technologies. In 2014, Wen *et al.* prepared fluorescent-magnetic double-coded nanospheres by layer-by-layer assembly method, and captured CTCs quickly, efficiently and sensitively.[56] Modified by the EpCAM antibody, the immunomagnetic nanospheres (IMN) successfully captured extremely rare tumor cells in whole blood, and the capture efficiency exceeded 94% after 5 minutes incubation. Wang *et al.* designed fluorescent-magnetic nanoparticles (F-MNPs) modified by double antibodies (targeting EpCAM and N-cadherin) for the efficient separation and identification of heterogeneous CTCs. In artificial samples mixed with MCF-7, HeLa and CCRF-CEM cells, the capture efficiency of F-MNPs modified by double antibodies was 99%, 81% and 0.63%, respectively.[57] Hu *et al.* synthesized a zirconium-based metal–organic-framework with dual antibody (anti-EpCAM and anti-N-cadherin) modified magnetic beads, and realized the capture and release of CTCs.[58] Xia *et al.* designed a double-targeted magnetic fluorescent bead MB-MLP-EpCAM, which realized the capture of CTCs and real-time monitoring *in vivo*.[59] This design has the characteristics of high accuracy, good selectivity and high resolution. The capture efficiency of CTCs is more than 85% and the cell viability is more than 90%. Based on the principles of gradient magnetic separation, fluorescence imaging and biomimetic membrane, Liao *et al.* designed biomimetic fluorescence-magnetic nanoprobes modified by different antibodies for the gradient magnetic separation of tumor cells in $BT474^{Her2++}$, $LNCaP^{PSMA++}$ and $MDA\text{-}MB\text{-}231^{Vim+}$ models.[60] The cell subsets bound by these nanoprobes were specifically identified and magnetically separated at different time points under external magnetic field. They demonstrated good capture performance within a few minutes, and the low detection limit of 1 cell per mL was achieved in blood samples.

The CTCs separation method based on immunomagnetic separation has made many improvements and breakthroughs in capture efficiency and purity, but the traditional preconcentration and detection method has the limitations of long detection time and tedious process. In recent years, the direct detection strategy of CTCs has received widespread attention. Wu *et al.* developed a cell-friendly one-step detection strategy based on immunomagnetic nanospheres (IMNs) and immunofluorescent nanospheres (IFNs).[61] The detection of CTCs in whole blood of 1 mL was achieved only after 20 minutes of incubation, with a capture efficiency of 98.1 ± 0.8%, a capture purity of 59.5%, and a good reproducibility. On the basis of this research, based on the capture performance of multi-functional nanospheres, a microfluidic platform based on spectrally combined encoding (SCE) was proposed to realize the multiple phenotypic analysis of a single CTC (Fig. 5A).[62] Different cellular biomarkers uniquely labeled by multi-functional nanospheres

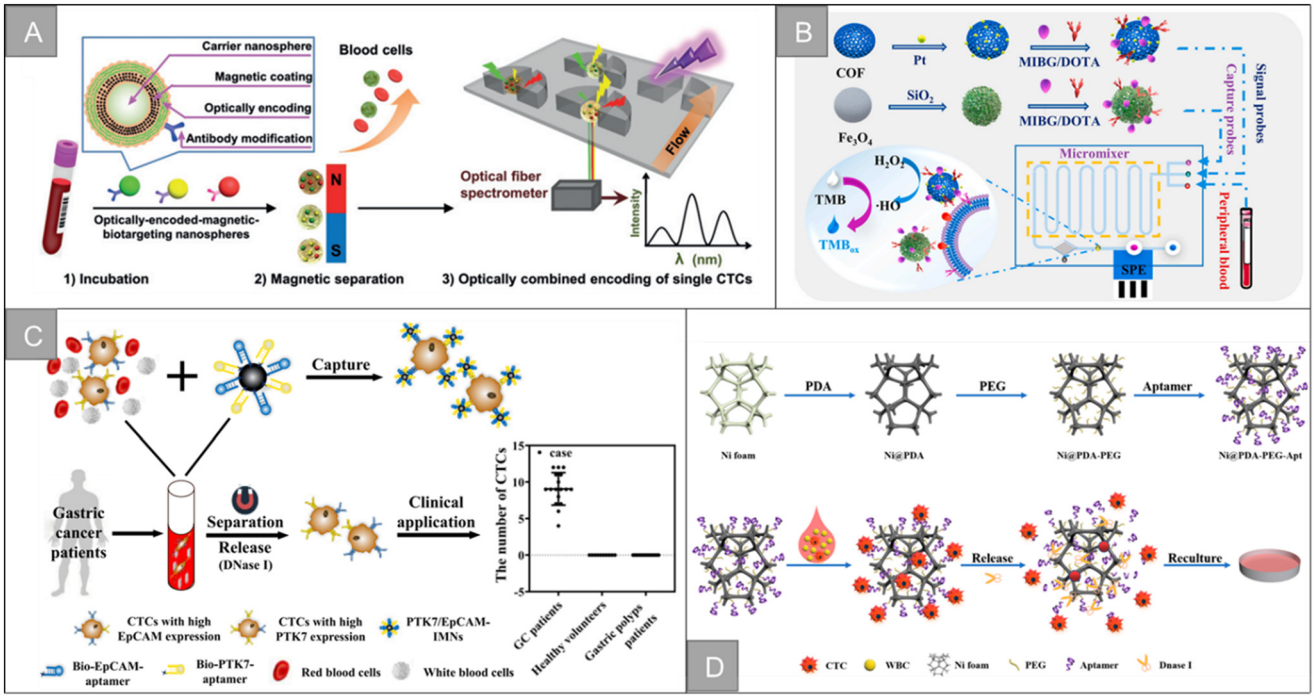

Fig. 5 Biological properties for isolation | (A) schematic diagram of a microfluidic chip with magnet[62] (reproduced with permission from ref. 62, Copyright 2020, John Wiley and Sons). (B) Schematic of the CTC capture, isolation, and quantification in the microfluidic chip[65] (reproduced with permission from ref. 65, Copyright 2022, Elsevier). (C) Schematic illustrations of the preparation of dual-aptamer-modified IMNs and its clinical application[21] (reproduced with permission from ref. 21, Copyright 2022, American Chemical Society). (D) Synthesis procedure of the Ni@PDA-PEG-Apt wafer, and capture and release of tumor cells with Ni@PDA-PEG-Apt wafer[75] (reproduced with permission from ref. 75, Copyright 2022, American Chemical Society).

bar codes have the same magnetic tags and different optical features, which can separate heterogeneous CTCs *in situ* with an efficiency of more than 91.6%, and quantitatively analyze the type and expression level of biomarkers by composite spectral characteristics. Guo *et al.* designed a supersensitive platform for the direct detection of CTCs using lanthanide fluorescence nanoprobes, which effectively avoided the interference of autofluorescence and the detection limit was as low as 1 cell per well in 96-well plates. The detection rate of blood samples from cancer patients (n = 15) was 93.9%.[63] Our research group combines the inverted microfluidic chip with immunomagnetic beads, and uses anti-EpCAM-Fe_3O_4@Ce6@silaneNPs to separate CTCs in the microcavity.[64] The capture surface of the microfluidic chip has a three-dimensional porous inverse opal structure and modifies the antibody. This increases the contact area with cells, while enhancing the ability of specific capture, and the capture efficiency is improved to 95%. In addition, the double-layer IOPC structure made of YVO_4:Yb^{3+} and Er^{3+} materials achieved 32-fold luminescence enhancement. The combination of the upconversion luminescence and immunomagnetic beads luminescence realized the real-time imaging of CTCs and real-time counting based on the fluorescence ratio. Liu *et al.* designed a dual-mode (electrochemical/visual) microfluidic device based on covalent organic framework (COF) to achieve the rapid and sensitive detection of PCC-CTC, as shown in Fig. 5B.[65] The device captures and recognizes the target CTCs by binding to the specific immunogenicity of the norepinephrine transporter and somatostatin receptor overexpressed on the surface of PCC cells. The detection time is 5 min, with a low detection limit of 1 cell per mL and a wide linear range of 2–10^5 cell per mL.

The nanoparticles camouflaged by the biomimetic cell membrane have ideal characteristics, which can resist homologous adsorption, improve the biocompatibility and enhance the targeting ability of materials, and have been widely used in various biomedical detection strategies. Rao *et al.* fused platelet (PLT) and leukocyte (WBC) membranes to form hybrid membranes, which were coated on magnetic beads, and then modified their surface with specific antibodies.[66] The PLT–WBC hybrid membrane is coated with immunomagnetic beads (HM-IMBs). HM-IMBs inherit the cancer cell binding ability enhanced by PLTs, reduce the adsorption of homologous WBC, and are further used for the efficient and highly specific separation of CTCs. Through the use of labeled blood samples, it was found that compared with commercial IMBs, the cell separation efficiency of HM-IMBs increased from 66.68% to 91.77%, and the cell purity increased from 66.53% to 96.98%. Wu *et al.* used white cell membranes to functionalize magnetic nanoparticles and modify antibodies on the surface of the membrane for the highly sensitive detection of CTCs.[67] The experimental results showed that the modification of the white cell membrane

effectively reduces the interference of homologous leukocytes, the capture efficiency of CTCs is increased to 96.82%, the capture purity is 90.68%, and the successful monitoring of clinical blood samples is realized.

2.2.2 Aptamer. Aptamers are a class of oligonucleotide sequences with specific recognition functions, which can be folded into specific three-dimensional structures and bind specifically to different biological targets with high affinity. In addition to the excellent binding ability of competitive antibodies, nucleic acid aptamers have the characteristics of simple synthesis, easy modification, stability and lack of immunogenicity, which make them an ideal alternative recognition candidate for biological detection.

Fang *et al.* designed a CTCs detection strategy combining upconversion nanoparticles and magnetic nanoparticles. In this study, aptamer-modified upconversion nanoparticles were used as a probe to identify tumor cells for the first time, and then enriched cells by attaching magnetic nanoparticles and stopping in a magnetic field to enhance the sensitivity of CTCs detection.[68] Li *et al.* developed a DNA template magnetic nanoparticles-quantum dots-aptamer copolymer (MQAPs) for the rapid magnetic separation of blood CTCs.[69] MQAPs can be detected in 20 min, the capture efficiency and purity are more than 80%, and can be used for single cell analysis. Wang *et al.* designed a fluorescence-open aptamer sensor FSC-D-P_0 for the sensitive detection of CTCs and tumor imaging. FSC-D-P_0 is composed of magnetic nanoparticles coated with two ssDNA and fluorescent P_0 aptamers, which has stable targeting and can be used for selective capture, MR/FL imaging and release of CTCs.[70] Li *et al.* designed a new type of anti-non-specific adsorption immunomagnetic platform Fe_3O_4@SiO_2@PTMAO@aptamer, which can efficiently capture different phenotypes of CTCs in 10 min, and briefly analyzed the relationship between different phenotypes of CTCs and the progression, diagnosis, surgery and chemotherapy of colorectal cancer (CRC) patients.[28] In addition, the team designed double aptamer (EpCAM and PTK7)-modified immunomagnetic Fe_3O_4 particles for the effective capture and downstream analysis of heterogeneous CTCs in patients with gastric cancer (Fig. 5C).[21] After 20 minutes of incubation, more than 95% of the MGC-803 and BGC-823 cells could be captured internally, and the prepared IMNs were successfully applied to CTC capture in peripheral blood samples of 1.0 mL patients with gastric cancer. Ding *et al.* combined aptamer-modified near-infrared fluorescent Ag_2S nanoparticles with immunomagnetic beads to design near-infrared fluorescence probes for efficient CTC capture, which greatly improved the imaging sensitivity.[71] On this basis, the research team designed the magnetic nanoparticles HM-Fe_3O_4@SiO_2 coated with the tumor cell membrane and leukocyte membrane by making use of the homologous repulsion characteristics of the white cell membrane and the homologous targeting ability of the tumor cell membrane.[72] It was then connected with multivalent aptamer-functionalized Ag_2S nanoparticles through the action of SA-biotin, which greatly improved the binding ability and anti-interference ability of the materials. The capture efficiency and purity of the CTCs are as high as 97.63% and 96.96%, respectively.

In addition to the traditional application of magnetic separation, a variety of cell detection strategies based on aptamers have emerged in recent years. Chen *et al.* designed a sensitive, simple and low-cost non-enzyme amplification CTCs detection strategy to achieve the uniform visual and fluorescence detection of A549 lung cancer cells in clinical blood samples.[73] Based on the selective recognition of Ag^+ and C–Ag^+–C by CdTe QDs, the detection limit of 3 cell per mL for A549 cells was detected by using mucin 1 as the CTCs marker and the aptamer as the recognition probe, and A549 cells with a mass concentration of 100 cell per mL could be identified by naked eye. Peng *et al.* designed electrochemical biosensors modified by double aptamers for the detection of specific CTCs in complex whole blood matrix.[74] Two aptamer hairpin probes can bind to two adjacent proteins (MUC1 and EpCAM) on the cell membrane, respectively, thus amplifying the electrochemical signal by rolling ring amplification reaction to achieve the sensitive quantification of specific CTCs, and the detection limit is as low as 3 cell per mL. Li *et al.* developed a low-cost and easy-to-manufacture aptamer-functionalized wafer Ni@PDA-PEG-Apt with three-dimensional (3D) interconnected porous structure (Fig. 5D).[75] It realized the rapid capture and release of CTCs in 1 hour. The 3D interconnected porous structure of the Ni@PDA-PEG-Apt wafer provides enough channels for cells to flow through and improves the contact frequency between aptamers and cells, with a high capture efficiency of 78.25% and a release efficiency of 61.85%. Wang *et al.* designed a CTC capture strategy based on a double aptamer DNA network that realized the efficient CTC capture, 3D encapsulation and CRISPR/Cas responsive release, which is helpful for downstream analysis of living cells (Fig. 6A).[76] Compared with the traditional cell enrichment strategy, the DNA network has higher capture efficiency and cell-friendly controlled release. The capture efficiency of the CEM cells and MCF-7 cells is 75% and 85%, respectively, and the post-60 min release efficiency is 80%. After 48 hours of culture, 91.8% of the cells have cell viability.

2.2.3 Peptide. Peptides play a key role in ligand–receptor and protein–protein interactions due to the recognition of short peptides that are mainly involved in the contact interface. In addition, the unique properties of small size, good stability, easy chemical synthesis, repeatability and large-scale production make peptides a very promising candidate for disease diagnosis, drug therapy and targeted drug delivery systems. Lu *et al.* designed a biotin-triggered decomposable immunomagnetic bead based on a short peptide sequence of Strep-tag II for the capture and release of CTCs.[77] The experimental results showed that the addition of biotin could release 70% of the captured cells, and 85% of the released cells were active. Bai *et al.* designed iron oxide magnetic nanoparticles Pep@MNPs functionalized by EpCAM recognition peptides, which achieved the same capture rate

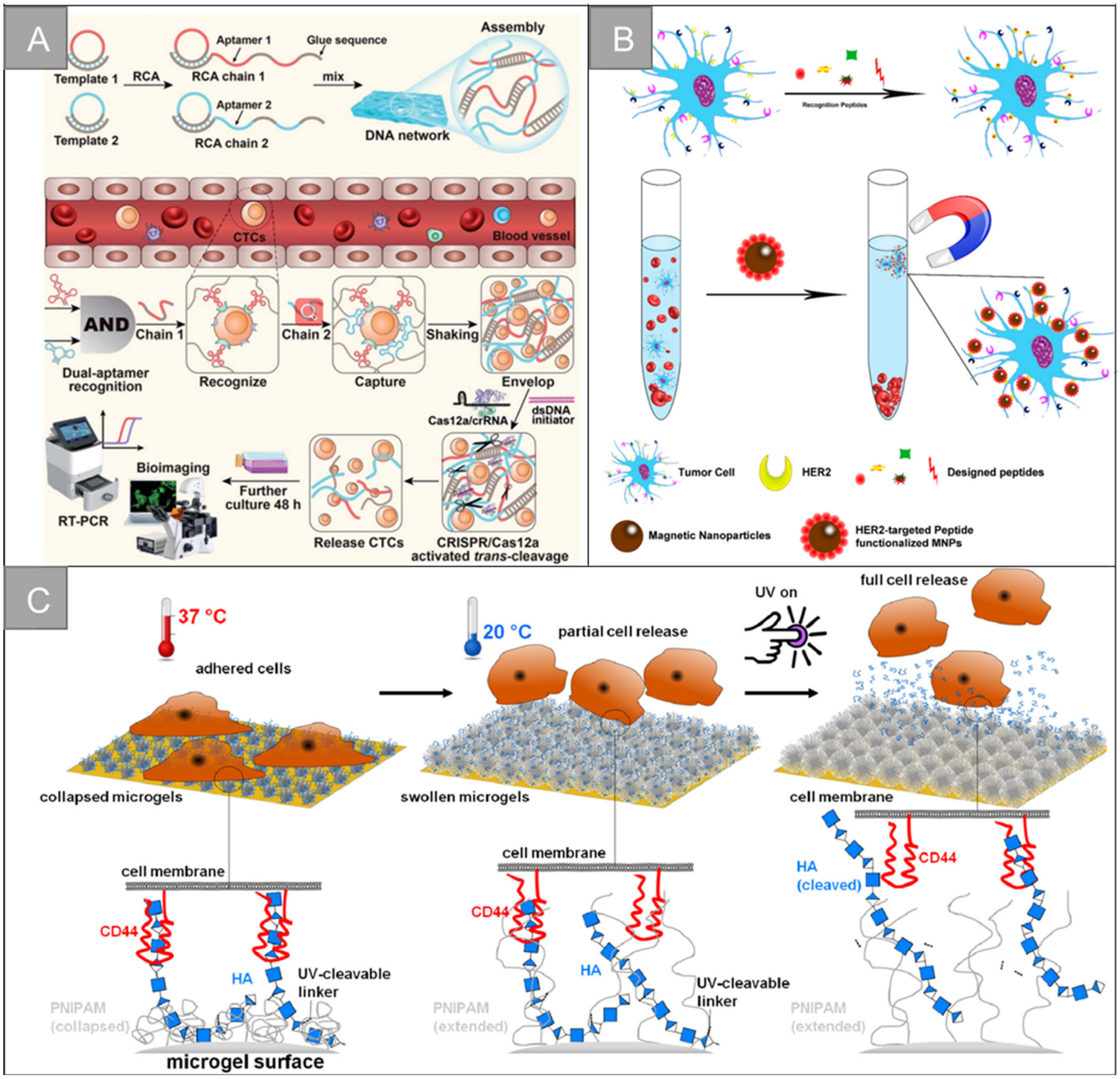

Fig. 6 Biological properties for isolation | (A) schematic of a CRISPR/Cas12a-responsive DNA network for CTC capture and release[76] (reproduced with permission from ref. 76, Copyright 2022, Royal Society of Chemistry). (B) Schematic illustration for HER2-targeting peptide screening and CTC isolation by Pep@MNPs[79] (reproduced with permission from ref. 79, Copyright 2017, American Chemical Society). (C) Illustration of the surfaces coated with dual-stimuli responsive HA-functionalized microgels and the expected cell release by temperature and light stimulus[93] (reproduced with permission from ref. 93, Copyright 2021, American Chemical Society).

(>90%) and capture purity (>93%) as EpCAM antibodies in artificial samples.[78] On the basis of this study, aiming at the problem that it is difficult to identify CTC subtypes, the research team designed and screened a peptide as a substitute for the HER2 antibody, and used peptide-functionalized magnetic nanomaterials to effectively isolate HER2 positive CTCs (Fig. 6B).[79] Jia *et al.* designed peptide-functionalized magnetic nanoparticles (NP@MNPs) based on N-cadherin targeting peptides, and combined them with EpCAM to recognize peptide-functionalized magnetic nanoparticles (EP@MNPs) to develop a CTC enrichment platform to enhance the recognition ability of different CTC subtypes.[80] The capture efficiency of mesenchymal CTCs was improved to 85%.

In addition, Han *et al.* designed an electrochemical biosensor for blood detection based on multifunctional peptides and the conducting polymer poly(3,4-ethylenedioxythiophene) (PEDOT).[81] Multifunctional peptides are assembled to the surface of the gold electrode by Au–S bond, which has the functions of anchoring, doping,

antifouling and recognition. Electrodeposition of PEDOT promotes the electron transfer at the sensor interface and improves the signal-to-noise ratio of detection, thus improving the sensitivity of the biosensor. The sensor has a wide linear range of more than 4 orders, and the detection limit is 17 cell per mL. Li *et al.* simulated the surface modification of folic acid (FA) and arginine–glycine–aspartic acid (RGD) peptides on the erythrocyte membrane.[82] The capture surface consists of a polydopamine layer, phosphorylcholine zwitterionic polymer and polyethylene glycol (PEG), which can repel 99.999% blood cell adhesion, effectively improve the enrichment ability of HeLa cells (19 000 times), and obtain high capture efficiency (91%) and high capture purity (89%) in labeled whole blood samples. Jiyoon Bu *et al.* developed a capture surface based on PD-L1-binding peptides to separate CTCs expressing PD-L1 from exosomes in the blood. This study examined the effects of the polyethylene glycol spacer, secondary peptide structure and peptide sequence modification on the capture efficiency.[83] The optimized pPD-1 configuration was 1.5 and 1.2 times more efficient than their total antibody counterpart (aPD-L1) in capturing tumor cells and exocrine expressing PD-L1, respectively. It showed that the common analysis of two biomarkers can further improve the accuracy of the clinical application of the system.

2.2.4 Chemical molecules. Folic acid (FA) can bind to the folate receptor (FAR) on the cell membrane with high affinity. The distribution of FAR is different in different tissues. It is almost not expressed in most normal cells and tissues, but overexpressed in a variety of cancer cells (ovarian cancer, colorectal cancer, pancreatic cancer, gastric cancer, prostate cancer, head and neck cancer, breast cancer and non-small cell lung cancer). Based on the differential expression of FAR and the high affinity of FA-FAR, FA has been widely used in individualized therapy, tumor imaging and cancer cell capture in the field of FAR positive cancer. Du *et al.* designed a simple, low-cost and efficient electrochemical impedance biosensor based on FA-functionalized zirconium metal organic framework FA@UiO-66 for cancer cell capture.[84] The sensor has good selectivity for FAR positive cancer cells, has good analytical performance in the linear range of 1×10^2–1×10^6 cells per mL, and the detection limit is 90 cell per mL. Hu *et al.* designed FA-biotin conjugates with different junctions to capture folate receptor positive (FR+) tumor cells mixed with whole blood.[85] Under the optimal design, the capture efficiency in PBS is close to 100%, and was successfully applied to the blood test of patients with non-small cell lung cancer, about 29 CTC/8 mL peripheral blood. Zhang *et al.* designed a biomimetic erythrocyte coating and modified DSPE-PEG-FA on the surface of the erythrocyte membrane by hydrophobic interaction to achieve the specific capture and release of circulating tumor cells with high expression of the folate receptor.[86] The strategy not only inhibits the non-specific adhesion of leukocytes, but also enhances the tumor targeting ability. The capture efficiency is more than 80%, the release rate is more than 70%, and the purity of tumor cells after release is more than 90%. Chen *et al.* used FA-modified T30 as a probe and used the double enzyme-assisted amplification strategy to analyze SMMC-7721 liver cancer cells from clinical blood samples by homogeneous fluorescence and color/distance two-dimensional vision analysis, which had the detection limits of 0.25 cell per mL and 1 cell per mL, and successfully applied it to the quantification of CTCs in clinical samples.[87] Wu *et al.* designed a surface-enhanced Raman scattering (SERS) biological probe based on TiO_2 for the sensitive detection of CTCs.[88] TiO_2 NPs were functionalized with alizarin red (AR), reduced bovine serum albumin (rBSA) and FA. It can be used to detect four different types of cancer cells. In addition, combined with the microfilter, the research team designed the FA-functionalized SERS biological probe B-TiO_2-AR-PEG-FA for single-resolution *in situ* separation and detection of CTCs.[34] The scheme improves the detection efficiency and accuracy, shortens the detection time to less than 1.5 hours, reduces the LOD to 2 cells per mL, and has been successfully applied to the detection of clinical blood samples.

Hyaluronic acid (HA) is a very rich polysaccharide in the extracellular matrix of all vertebrates, which can specifically target cancer cells that overexpress CD44 receptors. The CD44 receptor is overexpressed in breast cancer, prostate cancer, ovarian cancer, head and neck cancer, lung cancer and other cancer types, and tumor cells with a high expression of CD44 are more aggressive. Based on the specific recognition of HA and CD44 receptors and the high metastatic expression of CD44 cells, HA has great application potential in the fields of early tumor detection and drug therapy. Sun *et al.* designed silica magnetic beads with hierarchical structure to achieve efficient unlabeled cell capture.[89] Graded magnetic beads improve hydrophilicity, biocompatibility and stability through HA functionalization, with a high cell capture efficiency of 87.9–98.7%. Zhang *et al.* designed the HA-functionalized immunomagnetic nanomaterial Fe_3O_4@SiO_2-SS-HA, which realized the efficient capture and release of CTCs, benefiting from the high affinity between HA and CD44 overexpressed cancer cells.[90] The material can specifically capture CD44-overexpressed MCF-7 cells with an efficiency of 92%, and 81.4% of the captured cells were released after DTT treatment. Li *et al.* grafted dopamine onto the hyaluronic acid chain and developed a microsphere HA–DA for capturing CTCs overexpressed by CD44.[91] It has good selectivity and capture efficiency, and the detection limit is 10 cell per mL. Yin *et al.* designed the HA-functionalized silica coated magnetic beads HA-SiO_2@MBs, and combined it with a microfluidic chip to achieve the efficient capture and separation of CD44-overexpression cells.[92] The magnetic beads are specific to HeLa cells-overexpressing CD44 receptors, and the capture efficiency is as high as 92.0%. Melanie Schmidt *et al.* designed HA-functionalized double-response poly (*N*-isopropylacrylamide) (PNIPAM) microgel coating for CTC capture and release, as shown in Fig. 6C.[93] The HA-modified PNIPAM microgel

membrane can specifically capture the breast cancer cell line MDA-MB-231 expressing CD44, and the captured cells can be released by light stimulation and changing temperature.

Tannic acid (TA) is a widespread phenolic compound, which is composed of a large number of phenolic hydroxyl groups, catechol and galloyl groups. There is a strong hydrogen bond and hydrophobic interaction between the TA-containing galloyl group and glycolysis of tumor cells, which has excellent tumor-targeting ability. Moreover, TA shows good anti-leukocyte adhesion effect, which has great application potential in CTCs broad-spectrum capture. Yang *et al.* developed a simple and effective chemical strategy for capturing CTCs using TA functional membranes.[94] Because of the priority of the TA membrane over PBMCs to cancer cells, the membrane can effectively capture many types of cancer cells without the help of capture antibodies, the capture efficiency is greater than 76% and the capture cell viability is up to 90%. Ding *et al.* designed a simple broad-spectrum separation strategy for the effective separation of heterogeneous CTCs from blood samples using magnetic nanoparticles (MNPs)-functionalized by TA.[95] In the capture of artificial samples of seven kinds of cancer cells (HeLa, PC-3, T24, MAD-MB231, MCF-7, HT1080, A549), the capture efficiency of MNPs-TA is 62.3–93.7%. In addition, MNPs-TA was successfully used to test clinical blood samples from different cancer patients (n = 21). Zhou *et al.* designed a novel multi-functional platform based on double-response fluorescent magnetic Fe_3O_4/RhmB@ZIF-8-pTA nanoparticles (FR@Z-pTANPs) for the efficient separation and release of CTCs.[96] The platform has excellent resistance to the non-specific adhesion of leukocytes and high sensitivity to cancer cells in the patient's blood. It can capture more than 88% of EpCAM positive cells (MCF-7, HepG2) and EpCAM negative cells (MDA-MB-231, HeLa), and effectively releases captured cells with high efficiency (>80%) and survival rate (>90%) under cell-friendly pH/ATP stimulation. It provides a good solution to solve the challenge of heterogeneous CTCs in clinical application.

3 Nanostructure-based enrichment of circulating tumor cells

With the development of nanotechnology, nanostructured substrates have shown great potential in separating and detecting rare cells. Because the nanomaterials have similar sizes to the microvilli and pseudopodia on the cell surface, they can enhance cell adhesion according to the nano-topological interaction. In addition, nanostructured substrates have a larger specific surface area and provide more binding sites, which contribute to cell attachment. In recent years, a variety of nanostructures have been used for CTC enrichment based on the physical and biological properties of CTC. Besides 0-dimensional nanoparticles, 1-dimensional nanostructures (such as nanowires, nanorods, nanofibers), 2-dimensional nanostructures (such as nanosheets), various biomimetic nanostructure substrates and microfluidic chips for channel design based on hydrodynamics have emerged, which significantly promote the development of CTC enrichment technology.

3.1 Nanowire, nanopillar and nanorod

Silicon nanowires are generally obtained by chemical etching. The enhanced local morphology interaction between silicon nanowires and cell surface components (such as microvilli and filamentous pseudopodia) can effectively improve the efficiency of cell capture, and better CTCs separation can be obtained by cooperating with flow channel structure or immunomagnetic beads. Zhang *et al.* prepared layered assembled ITO nanowire arrays with horizontal and vertical nanowire branches, as shown in Fig. 7A, and the synergism between the terrain effect and specific molecular recognition significantly improved the detection time (35 min) and capture efficiency (89%).[97] Our team combines silicon nanowires with multi-functional magnetic nanocomposite Fe_3O_4@C6/Ce6@silane to design an inverted microfluidic chip to realize real-time monitoring of CTCs and *in situ* photodynamic therapy (Fig. 7B).[98] Under the action of composite markers and magnetic field, the capture purity of CTCs is increased to 90%, and the capture efficiency is 90.3%. Li *et al.* prepared a simple and highly selective bioseparation platform (A-BGC-SW).[99] For the recognition and release of CTCs in complex biological samples, A-BGC-SW used silicon nanowires (SW) as a substrate, amyloid bovine serum albumin (BGC) as coating and aptamer modification as the recognition group. Compared with natural bovine serum albumin (BSA), BGC-SW has a stronger surface interaction. The contamination of HAS, PRP and WBC is reduced by 88.5%, 88.0% and 83.7%, respectively. About 6 cells can be captured from a fresh blood sample containing only 10 CTCs per milliliter. Song *et al.* fabricated silver nanorod arrays by oblique deposition and modified double-tetrahedral DNA (DTDN) probes on their surfaces for the efficient capture, highly sensitive detection and lossless release of CTCs.[100] Under the best conditions, the capture efficiency of the biological interface is 90.2%. A total of 93.4% of the cells are released by Zn^{2+}-assisted DNAzyme cutting, and the survival rate of the released CTCs is about 98.0%.

Zinc oxide (ZnO) is a biocompatible metal oxide semiconductor material with excellent electrical, optical, mechanical and chemical properties, showing satisfactory performance in cell capture and release. Based on the characteristics, a variety of ZnO nanostructures, including nanowires and nanorods, have been widely used. Cui *et al.* grew ZnO nanowires vertically on the surface of a polydimethylsiloxane (PDMS) column substrate with gear structure to fabricate micro-nano biochips for the specific capture and lossless release of CTCs (Fig. 7C).[22] ZnO nanowires provide more binding sites and rough surfaces for capture. The capture rate of CTCs is more than 90%, the release efficiency is 93.95%, and the cell viability is 96%. Vahideh Shirmohammadli *et al.* designed a patterned highly vertical ZnO nanorod substrate to achieve the efficient

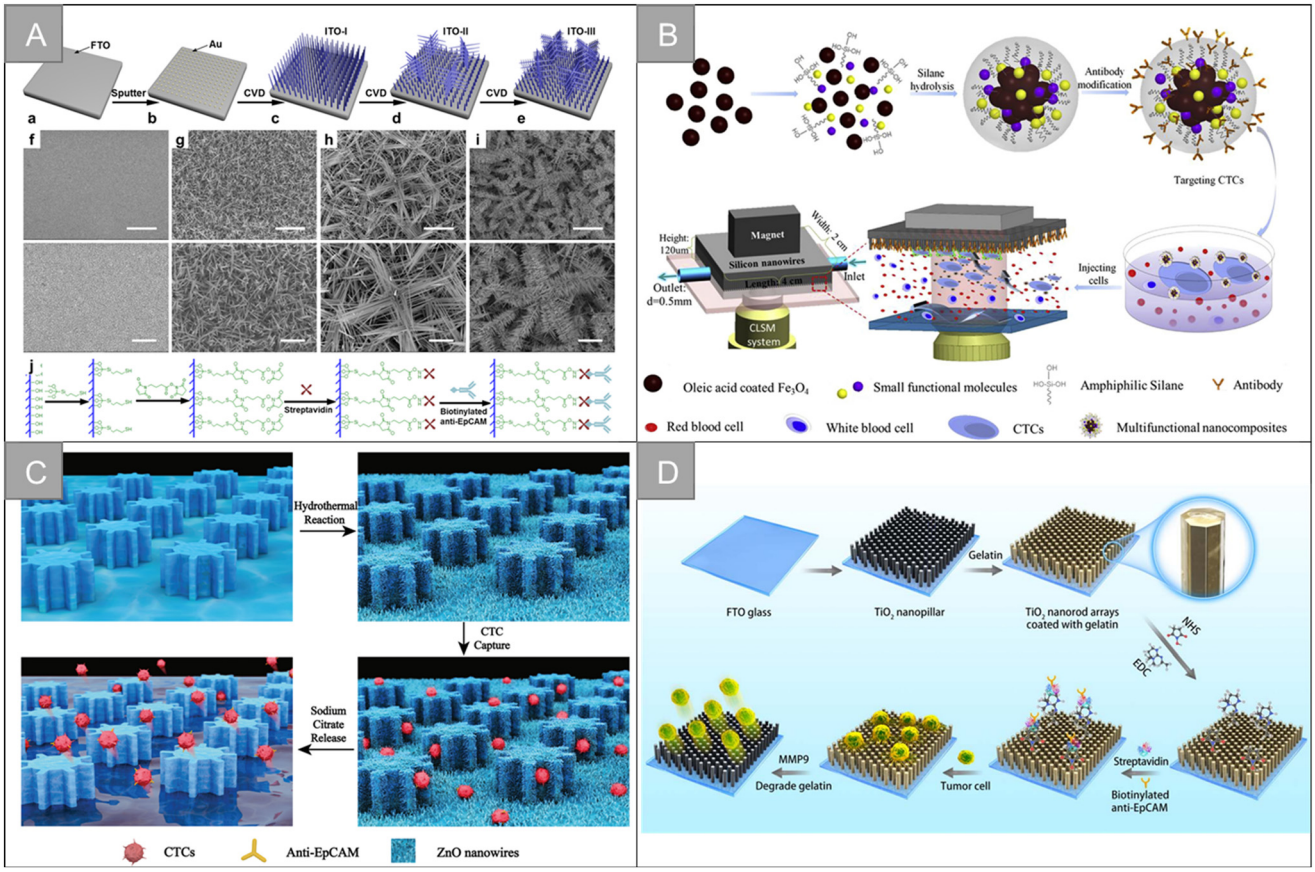

Fig. 7 Nanowire, nanopillar and nanorod | (A) schematic of the fabrication and functionalization of hierarchical ITO nanowire arrays on FTO[97] (reproduced with permission from ref. 97, Copyright 2016, American Chemical Society). (B) Schematic of the CTC capture platform, involving the synthesis of the anti-EpCAM-Fe_3O_4@C6/Ce6@silane nanocomposites and microfluidics chip under the confocal laser scanning system[98] (reproduced with permission from ref. 98, Copyright 2017, Elsevier). (C) Diagram showing a ZnO-coated G-PDMS pillar microchip for the capture and release of cancer tumor cells[22] (reproduced with permission from ref. 22, Copyright 2020, Royal Society of Chemistry). (D) Schematic of the modification of the TiO_2 nanopillar arrays (TNA) coated with gelatin film and conjugated antibody for the capture and release of circulating tumor cells[104] (reproduced with permission from ref. 104, Copyright 2019, IOP Publishing).

capture of two cell lines MCF-7 and MDA-MB-231, which adhere to different positions of the substrate, and the maximum capture efficiency is 98.4% and 86%, respectively.[101] Su *et al.* designed a 3D graphene macrocellular foam substrate with ZnO nanorod array.[102] Through the regular changes of electrical resistance and electrochemical impedance spectra of the foam substrate in the process of CTC adhesion, the specificity and non-invasive detection of CTCs were realized. Xu *et al.* constructed a sensing platform for CTC capture and detection based on CDS/ZnO nanorod arrays coated with polyaminophenylboric acid (APBA).[103] The sensing platform takes the terminal sialic acid (SA) molecule in CTCs as the recognition site, and realizes cell capture and release based on the regeneration of the ester bond between phenylboric acid and SA. It has good sensitivity and specificity in the concentration range of 50–1 × 10^6 cells per mL.

Titanium dioxide (TiO_2) has good stability, biocompatibility, and light transmittance. It is easy to modify the targeted molecules, so it is widely used in a variety of cell capture platforms based on nanostructures. Li *et al.* fabricated TiO_2 nanocolumn arrays coated with gelatin film to achieve the effective capture and lossless release of CTCs, as shown in Fig. 7D.[104] In this work, the interaction between the cell membrane and the nanostructure substrate improves the capture efficiency of CTCs up to 94.48%. The gelatin layer can be digested rapidly by matrix metalloproteinase-9 to achieve the lossless release of CTCs, with a release efficiency of nearly 100% and cell viability of 100%. Fan *et al.* coated a layer of gelatin film doped with gold nanorods on the TiO_2 nanorod substrate to achieve the efficient capture of CTCs and photocontrolled release in response to near-infrared light.[105] By adjusting the size and position of near-infrared light, selected cells can be locally released, while gelatin has good biocompatibility and low near-infrared phototoxicity so that the cells released by this method have high vitality.

3.2 Nanofiber

The nanofiber structure is a unique nano-structure imitating natural extracellular matrix, which has the characteristics of high specific surface area, high porosity, high mechanical

and structural stability. It provides a large number of active sites and enough contact area for cell capture and chemical reaction, and is an ideal platform for capturing circulating tumor cells. Chitosan is the most commonly used natural polymer material in tissue engineering because of its low cost, non-toxicity and good biocompatibility. Sun *et al.* prepared a functional biological interface based on chitosan nanofibers by electrospinning, which was used for the specific capture and lossless release of CTCs in blood.[106] The TiO_2 nanofiber is a widely used inorganic nanofiber material with the advantages of easy deposition, accurate control of size and bulk density. Chen *et al.* developed a platform for the sensitive capture and efficient sorting of CTCs based on the asparagine–glycine–arginine (NGR) peptide and TiO_2 nanofiber substrate.[107] As shown in Fig. 8A, the cell trapping of TiO_2 nanofibers densely arranged on the glass sheet provides a three-dimensional interface, which is conducive to enhancing the nano-topological interaction between the cell surface structure and the TiO_2 substrate. Subsequently, dopamine and bovine serum albumin (BSA) were introduced into the interface of TiO_2 nanofibers as adhesive and antifouling molecules for substrate surface modification. The formed TiO_2-BSA-NGR substrate has high capture sensitivity and efficiency, and the detection limit is 10 cells per mL, which provides a basic technical route for CTC capture.

Synthetic polymers have high flexibility in synthesis, processing and modification. Polyvinyl alcohol (PVA), polycaprolactone (PCL), polylactic acid (PLA), poly(lactic-*co*-glycolic acid) (PLGA) and other synthetic polymers are often used to design nanofiber substrates with different structural properties. In addition, compared with natural polymers, the mechanical properties of synthetic polymers can be effectively adjusted, and the economic benefits are better. Wu *et al.* assembled the aptamer targeting epithelial cell adhesion molecule and N-cadherin onto the PLGA nanofiber chip surface, and modified bovine serum albumin (BSA) on the chip surface to prepare an electrospun PLGA nanofiber chip for CTC capture of ovarian cancer (Fig. 8B).[108] The chip

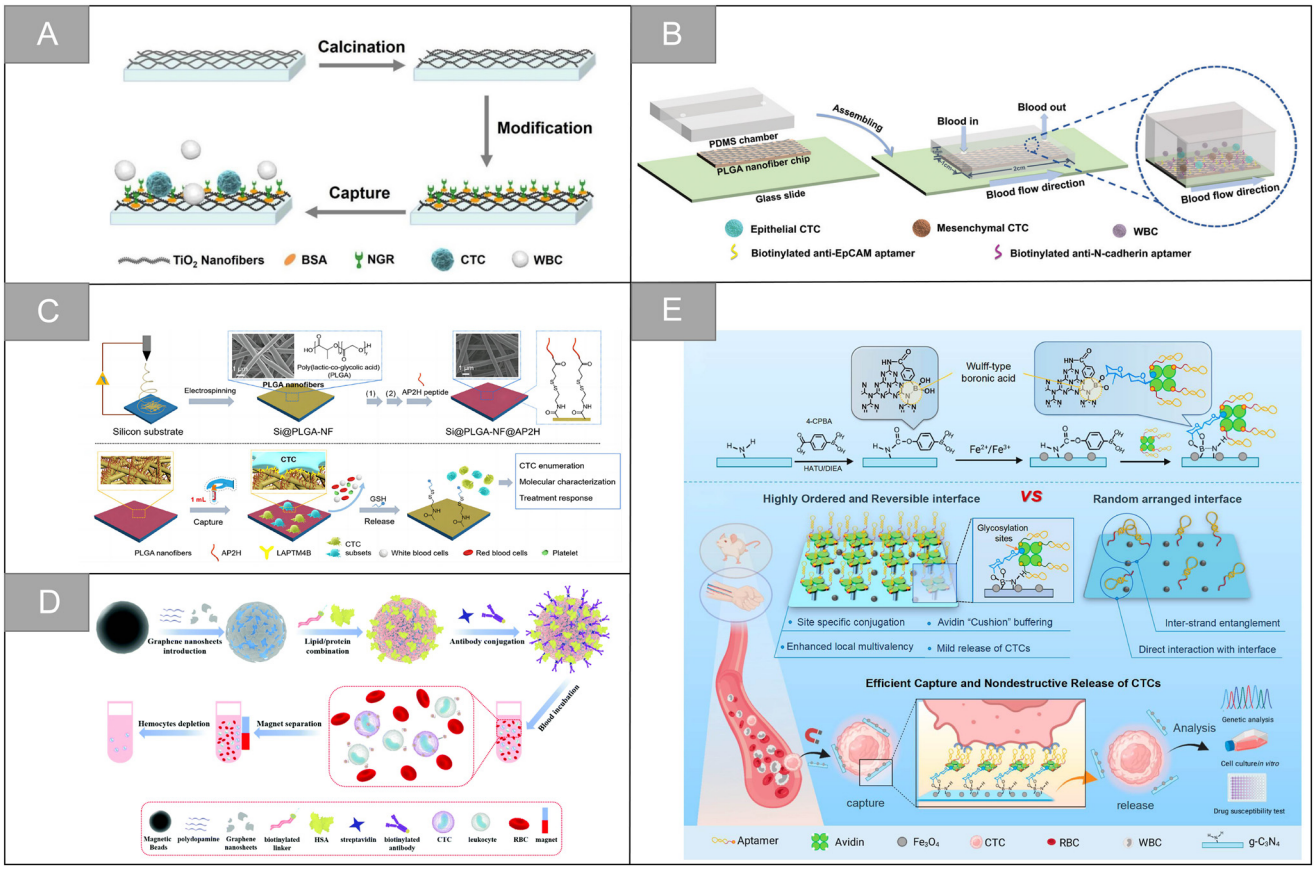

Fig. 8 Nanofiber and nanosheets | (A) schematic illustration of the CTC capture using the NGR peptide modified TiO_2 nanofiber substrate[107] (reproduced with permission from ref. 107, Copyright 2020, Springer Nature). (B) Schematic illustration of the dual aptamer-modified PLGA nanofiber-based microfluidic device for the different phenotypic CTC capture strategies[108] (reproduced with permission from ref. 108, Copyright 2021, Royal Society of Chemistry). (C) Schematic illustration synthesis and working principle of the Si@PLGA-NF@AP2H substrate[111] (reproduced with permission from ref. 111, Copyright 2021, American Chemical Society). (D) Schematic illustration of the fabrication process of artificial cell membrane-camouflaged immunomagnetic nanoparticles and general application in circulating tumor cell isolation[116] (reproduced with permission from ref. 116, Copyright 2022, Royal Society of Chemistry). (E) Scheme for the preparation of the CTC capture biointerface (Apt-Avi-BCN) and advantages of the highly ordered and reversible biointerface Apt-Avi-BCN with respect to randomly functionalized biointerface and its working principle for CTC capture and release[119] (reproduced with permission from ref. 119, Copyright 2022, American Chemical Society).

can improve the capture sensitivity and ensure the capture purity. The capture efficiencies of ovarian cancer A2780 cells and OVCAR-3 cells are 91% and 89%, and the release efficiency is 95% and 88%, respectively. Zhao *et al.* developed a simple method for CTC capture based on an electrospun PLA nanofiber substrate.[109] In this study, HA was modified on the surface of randomly or orderly electrospun polylactic acid fibers, which improved the hydrophilicity and blood compatibility of the PLA nanofibers. Experiments showed that ordered nanofibers had a higher capture efficiency of cancer cells with high expression of CD44 receptor, reaching 95.3%. Zhu *et al.* developed an aptamer-modified PEG–PLGA-nanofiber microfluidic chip.[110] The chip can be used for dynamic monitoring of CTCs mutation and rapid identification of rare subtypes, with excellent cell capture efficiency and high cell survival rate. The chip also has high application potential in dynamic CTCs counting, early tumor screening and histological change monitoring. Zhong *et al.* introduced lysosomal protein transmembrane 4 β (LAPTM4B)-targeting peptide as a new molecular target for the specific recognition of CTCs, and developed an amphiphilic and nanostructured platform for monitoring CTCs and capturing different CTC subtypes during treatment.[111] As shown in Fig. 8C, the platform uses an electrospun PLGA fiber scaffold as the base, utilizes the characteristic of high stable expression of the LAPTM4B protein during the epithelial-mesenchymal transition of CTCs, and uses the AP2H peptide as the recognition molecule to specifically capture tumor cells, which overcomes the limitation that some CTC subtypes are insensitive to traditional epithelial markers, and significantly enhances the capture affinity and selectivity. Wang *et al.* developed a negative microfluidic detection platform targeting WBC to solve the problem that cells must be labeled or attached to the substrate in the positive sorting method, which is difficult to release and culture.[112] In this research scheme, electrospun PLGA nanofibers were modified by streptavidin and embedded in a PDMS microfluidic chip. Through the interaction between biotin and streptavidin, the platform can sort the leucocytes labeled by biotinylated anti-CD45 antibody, and enrich CTCs and A549 cells from the blood of patients with non-small cell lung cancer. The leukocyte capture efficiency and cell recovery rate are ninety-seven percent and 97.5% respectively, which is an effective CTCs sorting and identification platform.

3.3 Nanosheets

Two-dimensional nanosheets are usually single-layer or laminated structures, which have the advantages of large surface area, flexible design, controllable morphology and excellent conductivity. Their surfaces can be modified with other materials, and their end groups are easy to functionalize, resulting in hybrid structures with enhanced electrical, catalytic or optical properties and detection capabilities, which are widely used in biosensing.[113]

Graphene oxide has unique optical properties, controllable size and easy surface modification with polyethylene glycol-based chemicals. It is an attractive nanomaterial in drug delivery and biosensing. In 2013, Hyeun Joong Yoon *et al.* designed functionalized graphene oxide nanosheets, which realized the effective separation of CTCs from blood samples of patients with pancreatic cancer, breast cancer and lung cancer, and the capture efficiency was 73 ± 32.4% at low concentration of target cells (3–5 cells per milliliter of blood).[114] Dou *et al.* synthesized a kind of aptamer functionalized and gold nano-array modified magnetic graphene nano-sheet, and realized multiple electrochemical detection of CTCs in blood.[115] The potential and current intensity of the probe respectively reflect the type and quantity of CTCs. In the detection of Ramos and CCRF-CEM cells, the detection limit is 4 and 3 cells per milliliter. As shown in Fig. 8D, Zhou *et al.* combined graphene nanosheets (GNS) with magnetic nanoparticles, and constructed antibody-modified artificial cell membranes on the periphery, which achieved the efficient capture of CTCs in simulated and clinical blood samples, with an average capture rate of 87.0%.[116]

Besides graphene oxide, other types of materials are widely used in the capture of circulating tumor cells based on nanosheets. You *et al.* designed and prepared a $Ti_3C_2T_x$-MXene nanosheets-near-infrared responsive gelatin hydrogel membrane for the specific capture and release of CTCs.[117] The surface of anti-EpCAM modified $Ti_3C_2T_x$@gelatin film can recognize highly specific EpCAM positive cells, and it has two release modes: temperature response release and near infrared response fixed-point release. The average effective release rate is 89%, and the cell vitality is 87%. Shen *et al.* developed an ultra-sensitive and specific sandwich cell sensor for detecting CTCs based on the aptamer-modified magnetic beads Apt@MBs and FA-functionalized carbon dot/cobalt oxyhydroxide nanosheet system FA@CDs/CoOOH.[118] Wang *et al.* developed a new cell capture interface based on boric acid-functionalized g-C_3N_4 nanosheets (Fig. 8E).[119] Compared with the free aptamer, the affinity of the engineered cell capture interface to the target CTCs is 100 times higher, and the captured CTCs can be released competitively through high-activity acidic fructose, which is beneficial to downstream cell culture and genome analysis, and further used for drug sensitivity test.

3.4 Bionic nanostructure

In addition to the imitation of mutual recognition between cells, there are many unique biological systems in nature. Compared with artificial systems, these systems have found their own ways to achieve the efficient recognition of specific targets. In recent years, a variety of biomimetic nanostructures have been constructed for CTC recognition. For example, pollen uses spiny structures to recognize and adhere to stigmas, and Wang *et al.* developed a biologically inspired pollen-like graded surface by assembling replicating

pollen grains.[120] After being modified with cancer cell-specific trapping agents, the pollen-like surface can capture target cancer cells with high efficiency and specificity, with an efficiency of 72.0% ± 1.5%. In addition, the pollen-like surface not only ensures the high viability of the captured cells, but also performs well in the cell mixing system and low cell density. Octopuses use long tentacles containing many suckers to hunt. Chen *et al.* mimicked the characteristics of the octopus and developed a device called "nano octopus" to isolate cancer cells in whole blood.[121] The device consists of magnetic particles (MP) imitating the head of an octopus and a long single-stranded DNA sequence anchored to the surface of the MP as antennae. Their ultra-high sensitivity and specificity are attributed to the multivalent binding of tentacle DNA to cellular receptors without steric hindrance. It has the characteristics of simple manufacturing, rapid detection, non-invasive capture and release, allowing a wide range of downstream cell culture and molecular analysis. Tabular corals have evolved long and flexible tentacles, allowing repeated "prickle cells" to maximize contact with flowing targets in a multi-valent way. Inspired by the efficient predation mode of plate coral, Jia *et al.* designed a multivalent nano-plate aptamer functionalized biomimetic magnetic graphene oxide platform (MNPA-TCMMGO), which combines the high binding affinity of polyvalent nucleic acid aptamers with the self-targeting and lateral fluidity of a tumor cell membrane to improve the recognition and capture ability of cancer cells in biological samples (Fig. 9A).[122] Inspired by the efficient predation mechanism of the sea urchin multitube foot and endoskeleton, Zhang *et al.* combined dual-multivalent-aptamers (DMAs) Sgc8 and SYL3C into AuNPs to form sea urchin-like nanoprobe sea urchin-DMA-AuNPs, and designed a super-efficient bionic single CTC recognition platform, as shown in Fig. 9B.[123] After co-incubation of CTCs and sea urchin-DMA-AuNPs, the separation is carried out by a microfluidic device integrated with a spiral separation unit and hydraulic filtration purification unit. After separation, by

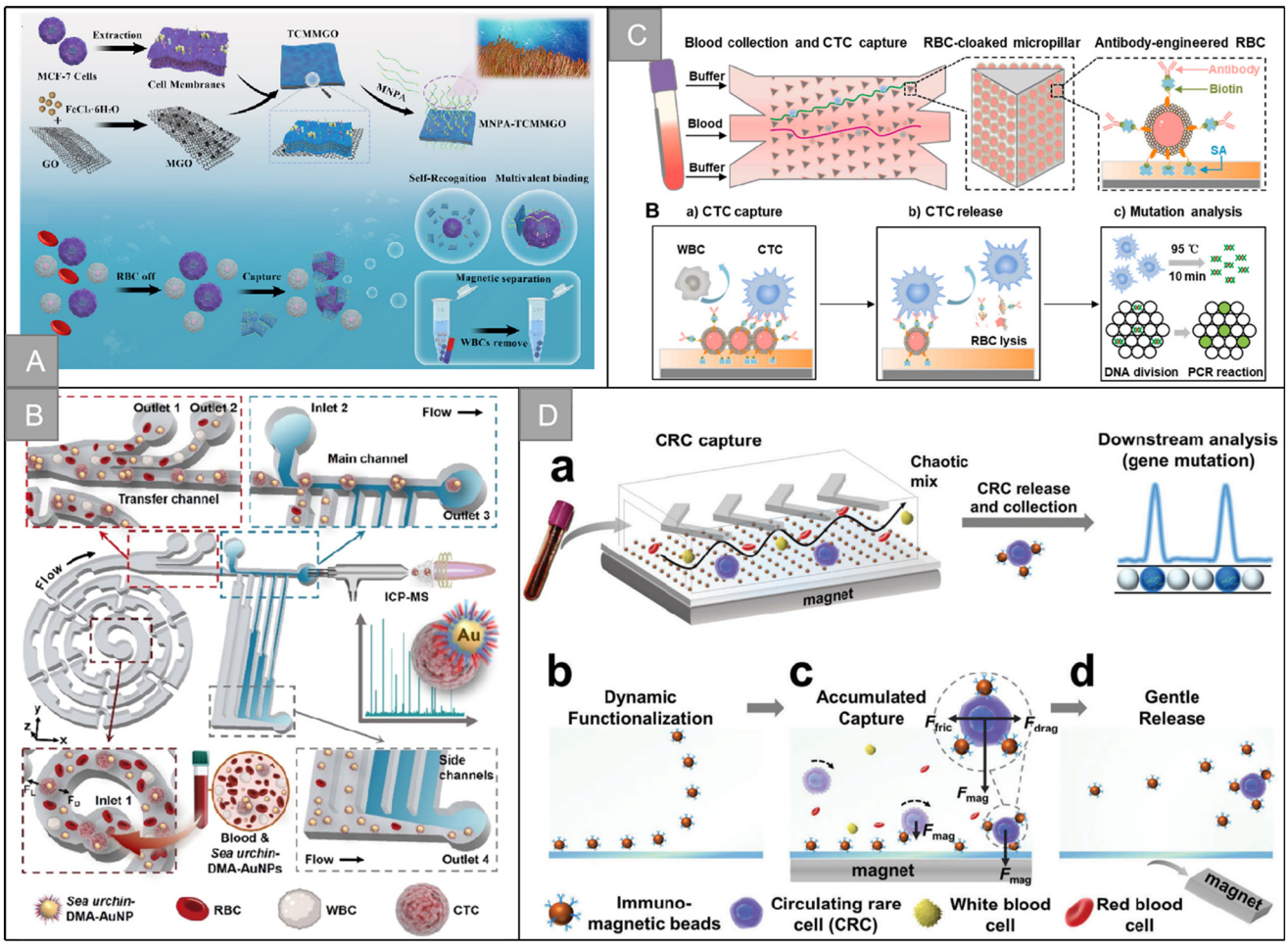

Fig. 9 Bionic nanostructure and micro-nano channel structure | (A) schematic illustration of the preparation of the MNPA-TCMMGO nanoplatform and MNPA-TCMMGO for the efficient isolation and detection of rare tumor cells[122] (reproduced with permission from ref. 122, Copyright 2023, Elsevier). (B) Schematic illustration of the dual-multivalent-aptamer-conjugated nanoprobes[123] (reproduced with permission from ref. 123, Copyright 2021, American Chemical Society). (C) Schematic illustration of the RBC-chip[127] (reproduced with permission from ref. 127, Copyright 2022, Elsevier). (D) Schematic illustration of the DynarFace-chip[131] (reproduced with permission from ref. 131, Copyright 2021, John Wiley and Sons (**https://www.wiley.com/**)).

measuring the amount of ^{197}Au isotope in sea urchin-DMA-AuNPs, the biomarker protein in a single CTC can be analyzed without background by inductively coupled plasma mass spectrometry. The microchip is helpful to identify a single CTC, and the separation rate is 93.6% at a flow rate of 60 μL min^{-1}. The measurement efficiency of a single CTC is 73.8 ± 5.0%.

Red rose petals are chosen as templates because of their microstructure size (the typical diameter of hemispherical micropetals is 20–30 μm) similar to CTCs, that promotes cell adhesion. In addition, many nanoscale folds are superimposed on these microstructures, which is beneficial for the cell pseudopod to grasp on the surface. Dou *et al.* prepared a hierarchical three-dimensional PDMS substrate composed of microcavities or microtops with nanostructured epidermal folds using rose petals as templates, and modified EpCAM antibodies on its surface for the effective capture and release of CTCs.[124] Compared with planar PDMS, there is a morphological interaction between the hierarchical structure and cells, which provides more sites for specific cell adhesion. The graded capture substrate shows 6 times higher cell trapping ability than a flat PDMS surface at the concentration of 100 cell per mL. The effective release of captured cells can be achieved by adding a GSH reducer. Wang *et al.* designed a biologically stimulated three-dimensional epithelial cell adhesion molecule (EpCAM) aptamer-modified rose petal-derived ZnO microchip EpCAM-RPD-ZnO-chip, which is used to achieve the efficient capture and release of CTCs.[125] The 3D rough spherical concave surface on the EpCAM-RPD-ZnO chip ensures the maximum contact with CTCs, and the capture efficiency is more than 90.5%. In addition, the simple release of ZnO was achieved by dissolving CTCs under moderately acidic conditions, with a release rate of 84.4% and a survival rate of more than 96.8%.

3.5 Micro-nano channel structure

Microfluidic technology, known as "lab on a chip", is a technology that accurately controls and manipulates micro-scale fluids, which is mainly characterized by the manipulation of fluids in the micro-and nano-scale space. It has the ability to miniaturize the functions of sample preparation, reaction, separation and detection in the process of biological, chemical and medical analysis to a few square centimeters of chip. In 2007, Nagrath *et al.* reported a breakthrough development of applying microfluidic chip based on a microcolumn array to CTC capture. Since then, many microchip technologies for CTC capture and detection have been proposed.[7]

In recent years, many works based on microfluidic channel design have been published, which has greatly promoted the development of *in vitro* detection of CTCs. Yang *et al.* designed a size-controlled microfluidic capture chip SDI-chip composed of triangular microcolumn arrays modified with EpCAM antibodies, which can make CTC fully contact with hydrodynamic optimized microcolumns.[126] The capture efficiency in blood samples is more than 92%, and the purity is 82%. In the subsequent work, the team combined the erythrocyte interface with deterministic lateral displacement (DLD) to establish an antibody engineering erythrocyte affinity interface (RBC-chip) on a microfluidic chip for the efficient separation and release of CTCs (Fig. 9C).[127] The erythrocyte layer reduces the collision between the cell and the microcolumn and avoids non-specific adsorption, and the capture efficiency of CTC is 96.5%. This work selectively cleaves RBC by simply changing the salt concentration, destroys the affinity interface, releases CTCs efficiently and gently, while avoiding nucleic acid contamination, and 96.1% CTCs maintain cell vitality. Mehdi Rahmanian *et al.* fabricated microfluidic chips with different geometric shapes (rhombus, rectangle, circle and triangle) microcolumns, and carried out numerical simulation and evaluation of the CTC capture efficiency and purity.[128] The experimental results show that the optimized diamond microcolumn has high capture rate (>85%), high purity (>90%) and high activity (97%). In addition, the diamond microcolumn chip was successfully applied to the CTC detection of 12 patients with breast cancer to verify the effectiveness of the chip.

Brenda J. Green *et al.* designed a dual-mode microfluidic device PillarX consisting of a series of cylindrical devices and X-devices, which can analyze a single CTC and cluster in whole blood according to the size, deformability and epithelial marker expression of a single CTC and cluster.[129] Larger, cohesive and less easily deformed clusters and larger individual cells are captured in the column device and classified according to the size of the column gap. Smaller, deformable clusters and individual cells are then captured in X-ray devices, and separated using functionalized magnetic nanoparticles according to the expression of epithelial markers. Aynur Abdulla *et al.* designed an antibody-functionalized microfluidic (AFM) chip for the rapid and accurate identification of CTCs in the whole blood of breast cancer patients.[130] The AFM chip consists of an entrance, an exit, three buffers and four parallel capture areas, including equilateral triangular columns and periodic curvilinear obstacles. The chip can effectively capture EpCAM-expressing cancer cell lines (MCF-7, PC3 and A549). At the flow rate of 0.6 mL h^{-1}, the capture efficiency reached 99.5%, 98.5% and 96.72% for MCF-7, PC3 and A549, respectively. The performance of the chip was evaluated with blood added by MCF-7, and the capture rate of the chip was 93%. Chen *et al.* designed a dynamic and reversible immunoaffinity interface (assembled by magnetic beads on the chip substrate by magnetic field) in the fishbone chip for efficient capture and release of CTCs (Fig. 9D).[131] The chip has the advantages of convenient operation and reversible assembly, the capture efficiency is more than 98%, and the released cell vitality is more than 98%. Elyahb A. Kwizera *et al.* designed a kind of electric microfluidic chip, which realized the efficient capture and release of heterogeneous (EpCAM+ and CD44+) CTCs.[132]

The VIZA chip has two entrances and five continuous bifurcated structures. The main channel consists of parallel patterned microcolumns. The surface of the microcolumns was first coated with 4 nm thick coupled titanium films and 10 nm Au films (except for the microcolumns in the four side columns), and then decorated on the gold surface to capture antibodies. In addition, the chip controls the movement of cells between the capture area and the non-capture area in the main channel by controlling the duration of the AC electric field, with a maximum capture efficiency of 97.0 ±

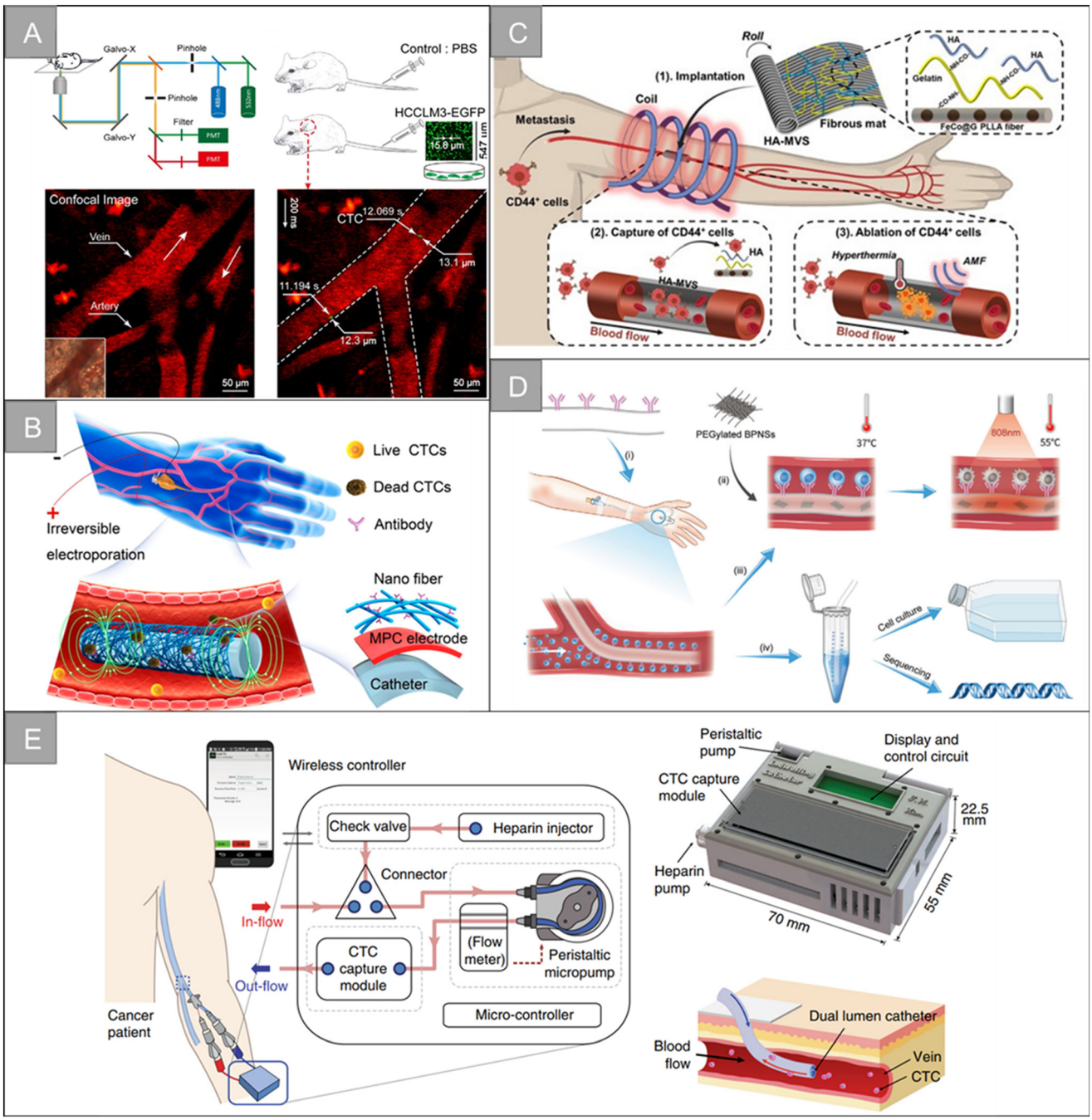

Fig. 10 Technologies for CTC enrichment *in vivo* | (A) schematic diagram of the setup of CTC detection by the confocal microscope system[23] (reproduced with permission from ref. 23, Copyright 2018, John Wiley and Sons). (B) Schematic diagram of the *in vivo* enrichment and elimination of CTCs using the flexible electronic catheter[151] (reproduced with permission from ref. 151, Copyright 2022, American Chemical Society). (C) Schematic diagram of the CTC removal by vascular-like ITD[152] (reproduced with permission from ref. 152, Copyright 2022, John Wiley and Sons). (D) Schematic diagram of the BPNSs-catheter based therapy[155] (reproduced with permission from ref. 155, Copyright 2020, John Wiley and Sons (**https://www.wiley.com/**)). (E) Schematic diagram the *in vivo* aphaeretic CTC isolation system[25] (reproduced with permission from ref. 25, Copyright 2019, Springer Nature).

0.8%. By injecting glutathione, the chip can achieve the efficient release of captured cells, with a release efficiency of 96.1 ± 1.2%.

4 Technologies for CTC enrichment *in vivo*

In vivo detection technology is an analysis method based on developing tumor cells that flow rapidly in blood vessels under physiological conditions. Because the tumor cells circulating in the body can be captured, even if the capture efficiency of the CTCs *in vivo* detection technology is as low as 0.02%, it is possible to detect one CTC in the body. In addition, it has many advantages, including the following: (1) it can dynamically monitor the changes in the number of CTCs in the patient's body in a formal physiological state; (2) it effectively avoids the influence of sample collection, pretreatment, transportation, storage, and other processes on the analysis results; (3) it is possible to capture CTCs from different parts of the body and different body fluids, which will promote a more comprehensive and accurate revealing of the tumor evolution process and mechanism, combining the subsequent molecular-level analysis. In recent years, *in vivo* detection technology has played a vital role in tumor staging, early detection, and predicting treatments' effects in metastatic cancer.

4.1 Fluorescence *in vivo* flow cytometry

The fluorescence-based *in vivo* flow cytometry (IVFC) is an emerging tool to monitor circulating cells *in vivo*. As a noninvasive and real-time diagnostic technology, the fluorescence-based IVFC allows for the long-term monitoring of circulating cells without changing their native biological environment.[133] Blood flow in the body is considered the fluid system of flow cytometry. When fluorescently labeled CTCs flow through the laser spot, the excited fluorescence is collected by a photomultiplier tube, producing a signal distinct from the blood background, enabling continuous, real-time, and long-term quantitative or qualitative analysis of CTCs. In 2004, the concept of *in vivo* flow cytometry (IVFC) was proposed for CTC detection.[134,135] Blood flow is considered to be the fluid system of the cytometer, and the laser is non-invasively focused into the blood vessel to excite fluorescently labeled CTCs. The fluorescence of CTCs passing through the laser focus can then be excited, collected, and detected *in vivo*. In 2007, the observation of fluorescently labeled CTCs in mouse blood vessels using high-power femtosecond laser line scanning on a two-photon microscope was reported.[136] In 2015, a specially designed fast-imaging confocal microscope was found to be able to capture images of injected cells, albeit at an insufficient imaging rate to capture all flowing cells.[137] In 2018, Hu *et al.* reported a simple optical method to directly monitor CTCs *in vivo* by ordinary confocal microscopy without additional modification or design (Fig. 10A).[23]

If the diameter of the vein (~80 μm) is too large compared to the CTC size (diameter: 10–20 μm), the CTCs may flow through the optical part of the scan line in the vessel. Therefore, such confocal line scans may miss those out-of-focus signals, resulting in reduced sensitivity of CTCs in whole vessels. However, confocal settings help suppress stray light from out-of-focus planes. The system then acquired each CTC signal with a higher signal-to-noise ratio. Fast line scanning with confocal microscopy enables continuous monitoring of CTCs in live mouse blood vessels for over 12 hours. In 2020, Patil *et al.* developed a new instrument called "*in vivo* diffusion flow cytometry" (DiFC) to count rare fluorescently labeled CTCs.[138] EC-17, a FITC-folate conjugate that has been used in clinical trials for fluorescence-guided surgery, showed high affinity for FR+ L1210A and KB cells *in vitro*. In whole blood, 85.4% of L1210A and 80.9% of KB cells were labeled with EC-17 over a nonspecific background, and EC-17-labeled CTCs were easily detected in the circulation of DiFC mice. In 2019, Ding *et al.* established subcutaneous tumor and orthotopic tumor models, and fluorescence *in vivo* flow cytometry was used to monitor the changes in the number of circulating tumor cells in the blood vessels of mice before and after tumor resection.[139] In the same year, Zhou *et al.* conducted label-free monitoring of melanoma cells *in vivo* based on the comparison of light absorption between melanin and other substances in blood in the near-infrared window.[140] A subcutaneous model of melanoma was constructed in the ear of mice to explore differences in the number of circulating melanoma cells (melanoma is the deadliest type of skin cancer) detectable in blood vessels distal to and proximal to the tumor. Non-invasive CTC detection in small animal models is possible using multiphoton fluorescence imaging. However, most of these techniques require labeling of CTCs by transfection, and their clinical translation is hindered by the low transfection efficiency *in vivo* and the potential toxicity of labeled CTCs. In addition, the penetration depth of this optical method is relatively shallow and can only act on superficial vessels, limiting the amount of blood to be examined within a reasonable operative time, thereby reducing detection sensitivity. Due to strong light scattering in biological tissues, some non-invasive optical CTCs imaging methods rely on imaging specialized anatomical sites, such as the mouse ear.

4.2 Photoacoustic imaging

Photoacoustic imaging (PAI) combines thermally induced acoustic waves generated by optical probing and ultrasonic (US) detection of a subject by irradiation with short laser pulses.[141,142] PAI allows the transfer of light energy absorbed by tissue, resulting in thermoelastic expansion. This expansion then generates ultrasound waves, which are detected by the transducer and produce a contrasting image of optical absorption within the tissue. Photoacoustic flow cytometry can achieve the signal recognition and counting of

different cells. It can identify the target signal in the background based on the specific absorption of the target signal to a specific wavelength. Different types and shapes of cells or nanoparticles have specific differences in the absorption of different wavelengths of laser light. Based on this difference, a single or multi-wavelength laser can be selected for excitation to determine the location and quantity to be detected.[143] Compared with fluorescence imaging, PAI has a centimeter-level penetration depth, can image surrounding blood vessels, and provides higher detection sensitivity by checking a relatively large blood volume at the same time. In 2020, Hai *et al.* used a linear array-based photoacoustic tomography system (LA-PAT) to detect melanoma CTCs, quantify their contrast-to-noise ratio (CNR), and measure their flow rates in most superficial veins in the human body.[24] This approach relied on the production of melanin within melanoma cells, rather than the expression of receptors on the cell surface. The development of contrast agents for molecular photoacoustic imaging may extend the capabilities of LA-PAT to image cancer cells that do not express melanin.[144]

However, PAI is facing some challenges in the clinical promotion. First, for cells that do not contain specific absorption substances, they need to be labeled with nanoparticles. The biological safety of these nanoparticles needs further study. Second, absorbers, including tissue and blood, act as a strong background for the PAI signal, severely reducing the specificity of detecting target molecules or cells, making it difficult to detect deeper blood vessels, and few CTCs in the effective vasculature in the early stages of cancer development. A new method called magnetodynamic photoacoustic (mmPA) imaging was developed to increase the specific contrast in PAI by suppressing background signals from intrinsic absorbers.[145–148] mmPA senses objects labeled with composite particles combined with paramagnetic nanoparticles and optically absorbing components (*e.g.*, gold nanorods), enabling magnetic manipulation to simultaneously target objects PA detection. By biocoupling the contrast agent to the target tissue or cells and magnetically manipulating it with an external magnetic field, the target region moves coherently with the magnetic field. This motion modulates the PAI signal spatially or temporally, allowing subsequent motion filtering of a series of recorded PA signals to suppress the magnetically insensitive background signal.[145,146,148]

4.3 Long term large blood volume scan

The low throughput of *in vitro* detection and the demand for a large number of CTCs in downstream analysis have promoted the development of CTC detection *in vivo*. In 2012, CellCollector, the world's first CTC *in vivo* capture product, was certified by CE and is currently the only *in vivo* CTC capture technology on sale that has been certified by CFDA. CellCollector technology inserts the wire coated with EpCAM into the elbow vein of the patient to collect CTC, which is taken out after 30 min, and the blood volume is up to 1500 mL, which is much higher than *in vitro* detection. In 2018, Vermesh *et al.* developed a flexible intravascular magnetic line MagWIRE for higher yields to retrieve rare biomarkers from the subject's *in vivo* blood.[149] MagWIRE is an independent magnetic line, which has the characteristics of small diameter, good flexibility and good biocompatibility. It can achieve a high local field gradient in its whole length to effectively capture magnetic particles (MP) coated with injected antibodies in the target labeled in the blood. In the *in vivo* capture experiment of pig ear vein, although the highest capture efficiency of MagWIRE is 8%, the number of cells captured is equivalent to 80 tubes of blood extracted *in vitro*, which is 5000 times higher than that of passive immune capture *in vivo*. Cheng *et al.* designed an injectable and retractable flexible three-dimensional stent CTC-Net for intravascular collection of CTCs.[150] CTC-Net has an interconnected spatial distribution network, which can hold a large number of fixed antibodies and increase the frequency of contact with cells. CTC-Net can be easily compressed and injected into blood vessels, and fully expanded to form a 3D "fishing net" structure for capturing CTCs. Dozens of CTCs have been successfully isolated and detected from tumor-bearing rats. In addition, the CTC-Net can be recompressed and retracted from the blood vessels to facilitate imaging and downstream analysis of the captured CTCs. As shown in Fig. 10B, Wang *et al.* combined electrospun nanofibers with liquid metal–polymer conductor (MPC) electrodes to develop a flexible electronic catheter that can efficiently capture and kill CTCs *in vivo*.[151] The catheter can repeatedly screen the blood of the whole body and has good flexibility, mechanical strength, biocompatibility and electrical conductivity. It enhanced specific recognition and cell adhesion by surface-modified epithelial cell adhesion molecules of nanofibers. The number of leukocytes captured per square millimeter catheter is less than 10, and the capture efficiency is much higher than that of previous studies. In addition, the CTCs concentrated on the surface of the catheter was finally ablated by irreversible electroporation (IRE), which effectively reduced the content of CTCs *in vivo* and reduced the damage of normal tissue, providing a new method for the capture and elimination of tumor metastasis and prognostic markers such as CTCs and exocrine. As shown in Fig. 10C, Yin *et al.* proposed for the first time a vascular integrated trapped device (ITD), which is an implantable HA modified magnetic vascular stent (HA-MVS) for the permanent capture and magnetothermal ablation of CD44 positive (CD44+) CTCs under an alternating magnetic field (AMF).[152] The HA-MVS can capture CTCs repeatedly in a dynamic environment (flow rate = 5.0 mL min^{-1}). In the setting of extracorporeal closed-loop circulation, the capture efficiency reached 21.6 ± 1.5% after 120 cycles, and 13.26 ± 4.22% in rats after 3 hours of *in vivo* circulation. Moreover, the heat generated by HA-MVS under AMF can destroy the cell membrane and induce apoptosis, resulting in 91.3% of CTC death.

Intravenous indwelling needle, which is widely used clinically, is a good framework for the construction of CTCs. Zhang *et al.* proposed the *in vivo* capture of CTC based on surface-modified intravenous indwelling needle transfusion.[153] When the needle is used for intravenous infusion, CTCs is captured at the same time, which will not cause further physical harm and reduce the invasion of *in vivo* detection. Li *et al.* designed a medical needle coated with ZnO nano-flowers for the capture and killing of CTCs.[154] *In vivo* and *in vitro* experiments showed that about 90% of the captured CTC was killed and fell off the surface of the needle after death, enabling the ZNFs needle to continuously remove CTCs.

The catheter is usually made of polyurethane, which can be covalently modified with tumor-specific antibodies to capture CTC in the blood. In addition, due to its long indwelling time in vessel, a large amount of blood continuously flows through the surface of the retention needle with the aid of circulation. This greatly increases the contact rate between the cells in the blood vessel and the marker, which can effectively increase the capture efficiency. Wang *et al.* developed a minimally invasive therapeutic intravenous catheter (Fig. 10D) for *in vivo* enrichment and photothermal killing of CTCs.[155] The surface of the catheter was modified with anti-EpCAM antibody and the interior was filled with black phosphorus nanosheets (BPNS). CTCs in peripheral blood are continuously captured by the catheter with the help of circulation. Captured CTCs are used for downstream analysis or eliminated *in vivo* by the near-infrared (NIR) photothermal effect of BPNS. A capture efficiency of 2.1% was obtained during a 5-minute treatment, and 100% of the captured CTCs were killed by NIR light irradiation in an *in vitro* closed-loop circulatory system and in an *in vivo* rabbit model. Kim *et al.* described an indwelling intravascular non-circulating CTC isolation system (Fig. 10E) to continuously collect CTCs directly from peripheral veins.[25] A patient may wear the device for hours, and a relatively large amount of blood can be examined through the device. The system consisted of four main parts: a microcontroller, a peristaltic pump, a heparin injector, and a CTC capture module containing a microfluidic CTC capture chip. The system was designed to accommodate any type of CTCs isolator, as long as it is configured to fit the system manifold. The system allowed for periodic CTCs assessment by exchanging CTCs collection chips, while continuously monitoring blood flow. It could accommodate any type of CTCs separation device, as long as it was compatible with the system's manifold. The design of the interchangeable CTC chip solved the device blocking problem expected from saturation of the CTC capture module in the CTC capture module. This means the system can be left in place for longer periods of time, potentially allowing large blood samples to be interrogated with little harm. This allows for adequate patient mobility during surgery, and minimizes patient inconvenience. It is worth noting that the capture module currently used in this system is designed for CTC-immobilized EpCAM, which can be obtained by combining with other antibodies or aptamers or equipped with physical structures for higher capture efficiency.

In total, there has been little work on the *in vivo* enrichment of CTC based on nanostructures. Due to the complexity of the *in vivo* environment and the characteristics of CTC itself, the published research work, such as intravascular magnetic lines, temporary retention system, *in vivo* enrichment and killing of CTC, have further enriched the enrichment means of CTC, and explored the feasibility of CTC intervention *in vivo*, which have received great attention. However, the remarkable results have not been achieved. The low efficiency and the biosafety of *in vivo* capture still restrict the development of *in vivo* enrichment technology. Judging from the existing research, it is a possible development direction to improve the capture efficiency and detection efficiency based on *in vivo* intervention. In addition, the problems derived from *in vivo* capture technology, such as feasibility and safety, need further exploration by researchers.

5 Downstream analysis

With the progress of technology, the study of CTC has changed from simple counting to the era of molecular typing and genotyping. Because CTC is very rare and mixed in many peripheral blood cells, separating CTC from white blood cells, red blood cells, and other blood components is an indispensable step in CTC research and downstream analysis. Capture efficiency and capture purity are the two most basic indicators to evaluate the CTC enrichment technology platform. The enrichment platform with high capture efficiency can avoid the missed detection of CTC in samples to the greatest extent. That is, it has excellent peripheral blood CTC detection ability and detection rate. The enrichment platform with high capture purity maximally avoids the interference of other components (mainly white blood cells) in peripheral blood. It ensures the purity of genetic material extracted in downstream analysis. In addition, whether CTC can maintain high cell viability after release, the detection rate of authentic samples, and the number of captured CTC all affect the clinical application of CTC.

With the development of new capture technology, the capture performance of CTC was dramatically improved. Recent CTCs enrichment strategies based on nanostructures and fundamental indicators are shown in Table 1. CTCs obtained by various enrichment methods are usually further processed for downstream analysis. The most commonly used methods for specific identification and downstream analysis of CTCs include tumor-specific antigen detection based on immunocytochemistry/immunofluorescence staining and various molecular analysis methods based on nucleic acid sequence identification (fluorescence *in situ* hybridization FISH, array comparative genomic hybridization aCGH, next-generation sequencing NGS, polymerase chain reaction PCR). Compared with ctDNA, capturing CTCs is relatively tricky. However, it has a complete cell morphology, which can be used for morphological and functional observation, and

Table 1 Summary of CTC enrichment methods based on nanostructures

Category	Methods	Cell lines	Cell line isolation result			Clinical blood sample or animal model				Ref.
			Yield	Purity	Viability	Ratio	CTC count			
Physical properties for isolation										
Size and morphology	Ultrathin Si_3N_4 filtering membrane with slit-shaped pores	A549, HCT-116	*C*: 96%	99.99%	90%	100% (n = 10)	6–20 cells			20
	Cluster-Wells microfluidic chip	HeyA8, LNCaP, MDA-MB-231, MCF-7	*C*: 93.2%, *R*: 96%	99%	95.8%	75% (n = 10) and 88.9 (n = 10)	0.063 to 0.867 clusters per mL, 0.167 to 59.2 clusters per mL			36
Density	Fully automated, negative depletion-based continuous centrifugal microfluidics	A549, PC9, H1975, MDA-MB-231, SK-BR-3, T24	*C*: 92%, *R*: >90%	99.9%	—	100% (n = 30)	12–120 cells			39
Electrical properties	Microwells fabricated on interdigitated electrodes	DU-145	*C*: 90%	—	—	—	—			43
Acoustic properties	Initial acoustofluidic preseparation and negative selection acoustophoresis	DU145	*C*: 94%, *R*: 42%	99.5%	96.8%	—	—			47
Fluid mechanics	A miniaturized centrifuge with four paralleled inertial spiral channels with a two-stage serpentine channel	MCF-7, A549	*C*: 86.5%	93%	—	—	—			53
Biological properties for isolation										
Antibody	Luminescent lanthanide nanoprobes	MCF-7	*C*: 93.9%			—	—	93.9% (n = 15)	10–190 cells	63
	Nanoprobes with gradient magnetic response	BT474, LNCaP, MDA-MB-231	*C*: 90.2 ± 2%			92.1 ± 2.4%	—	—	—	60
Aptamer	Multivalent aptamer functionalized Ag_2S nanodots and hybrid cell membrane-coated magnetic nanoparticles	MCF-7	*C*: 97.63%			96.96%	—	100% (n = 8)	6–10 cells per mL	72
	Dual-aptamer-modified immunomagnetic particles	MGC-803, BGC-823	*C*: 95%			—	—	100% (n = 17)	4–12 cells per mL	21
Peptide	EpCAM recognition peptide functionalized iron oxide magnetic nanoparticles	MCF-7, SK-BR-3, PC3, Hep G2	*C*: 90%			93%	—	—	—	78
Folic acid	FA-functionalized bionic layer of RBC	HeLa, HCT116	*C*: >80%, *R*: >70%			90%	>90%	100% (n = 5)	3–21 cells	86
Hyaluronic acid	HA-functionalized redox responsive immunomagnetic nanocarrier	MCF-7	*C*: 92%, *R*: 81.4%			—	—	—	—	90
Tannic acid	Dual-responsive fluorescent-magnetic nanoparticles	MCF-7, HepG2, MDA-MB-231, HeLa	*C*: >88%, *R*: >80%			86.9%	>90%	100% (n = 15)	3–30 cells per mL	96
Nanostructure										
Nanorod	Double-tetrahedral DNA probe functionalized Ag nanorod biointerface	SGC-7901	*C*: 90.2%, *R*: 93.4%			—	98%	—	—	100
Nanofiber	Dual aptamer-modified PLGA nanofiber-based microfluidic devices	A2780, OVCAR-3	*C*: 91%, *R*: 95%			—	>90%	100% (n = 7)	1–13 cells per mL	108
Nanosheets	Boronic acid-functionalized g-C_3N_4 nanosheets	HepG2, SK-HEP-1	*C*: 97.64%, *R*: 99.17%			99%	98%	100% (n = 20)	5–43 cells per mL	119
Bionic nanostructure	Bioinspired 3D aptamer modified rose petal derived ZnO microchip	MCF-7, PC9, A549	*C*: 90.5%, *R*: 84.4%			94%	96.8%	100% (n = 21)	3–36 cells per mL	125

Table 1 *(continued)*

Nanostructure								
Micro-nano channel structure	Antibody-engineered red blood cell affinity interface on microfluidic chip and DLD-patterned interaction model	SW480	*C*: 96.5%, *R*: 96.9%	—	96.10%	100% (n = 20)	2–58 cells per mL	127
	A robust microfluidic chip containing virtually implemented zones surface-coated with gold	MCF-7, MDA-MB-231, MDA-MB-468	*C*: 97%, *R*: 96.1%	—	>90%	100% (n = 60)	4–187 cells per mL	132
In vivo enrichment of CTC								
Venous catheter	Indwelling intravascular aphaeretic system	MCF-7	*C*: 1–2% (2 h)	—	>90%		762 cells in canine blood	25
	Black phosphorus and antibody functionalized intravenous catheter	HepG2	*C*: 2.1% (5 min), *D*: 100%	—	—		2100 cells in rabbit blood	155
	HA-modified magnetic vascular scaffold	MDA-MB-231	*C*: 13.26 ± 4.22% (3 h), *D*: 91.3%	—	—		132 600 cells in rat blood	152

C, capture efficiency; *R*, release efficiency; *D*, death rate.

include complete genetic information such as proteome, transcriptome, and genome. In addition to CTCs counting, the analysis of CTCs helps identify specific molecular targets related to treatment, expanding people's understanding of basic molecular pathways related to invasion, migration, and immune surveillance, identifying more invasive tumor cells and promoting the development of personalized therapy.

5.1 Disease detection and prognosis evaluation

The prognostic value of CTCs has been confirmed in a variety of cancers. In addition, the value of CTCs in early detection of solid tumors, efficacy and disease recurrence monitoring has been gradually recognized. In recent years, based on a variety of emerging technologies, there has been a lot of research work on the use of CTCs in disease detection and prognosis evaluation. Wan *et al.* made a maze microfluidic device to effectively separate CTC from peripheral blood of patients with HCC, and studied the correlation between the number of CTCs and clinical HCC stage.[156] In this work, blood samples from 42 HCC patients were selected and compared with 5 non-HCC healthy subjects. CTCs were identified in 88.1% of HCC patients at different tumor stages. The statistical results showed that a higher positive rate of CTCs was found with the later HCC stage. In addition, 55% of the patients had circulating tumor microthrombus (CTM), which was also related to the late HCC stage. Based on the immunomagnetic platform Fe_3O_4@SiO_2@PTMAO@aptamer, Li *et al.* detected the number of epithelial CTC (E-CTC), stromal CTC (M-CTC) and mixed (epithelial and stromal) CTC (EM-CTC) in blood samples of patients with colorectal cancer, and analyzed the correlation between different phenotypes of CTCs and clinical information of CRC patients.[28] The changes of the proportion of heterogeneous CTC in 40 patients with different stages of colorectal cancer before and after operation showed that the number and proportion of E-CTC or M-CTC was significantly lower than that of EM-CTC and M-CTC. This was positively correlated with the metastasis of colorectal cancer and the effect of operation and chemotherapy in patients with CRC. The proportion of M-CTC decreased in all stages after operation, but only in advanced patients. Based on the multi-functional nano-delivery system, Ren *et al.* realized genome editing and *in situ* evaluation of therapeutic response to *in vitro* CTCs at the single-cell level, providing accurate information for personalized cancer treatment.[157] In this study, C-X-C motif chemokine receptor 4 (CXCR4), a typical target protein in cancer therapy, was selected as the representative target for genome editing *in vitro*. Single cell analysis showed that CXCR4 in CTCs of cancer patients was effectively downregulated, anti-cancer biomarkers such as p53 and p21 were upregulated, and the edited cancer cells showed inhibition of proliferation and inhibition of migration and invasion. Using the same targeted delivery vector to deliver molecular beacons to the liver, the therapeutic efficiency of cancer cell lines and genome editing in CTCs can be easily detected.

5.2 Gene analysis and auxiliary targeted treatment

Molecular targeted therapy based on tissue biopsy is a typical case of cancer precision medicine. Although tissue biopsy can accurately obtain tumor genetic information, tissue biopsy is an expensive, invasive and painful process. Only some tumor sites can be sampled regularly. Obtaining tumor cells from blood sampling or liquid biopsy is a promising alternative to tumor biopsy. In recent years, CTC gene mutation profile analysis, as an auxiliary diagnostic tool, has been used to characterize tumor molecular heterogeneity and tumor genotype monitoring to guide treatment because of its low invasion, carrying primary and metastatic tumor characteristics and complete genetic information.

Cheng *et al.* proposed a large-scale parallel analysis of hydrodynamics single-cell RNA sequencing (scRNA-seq) bar code technology Hydro-Seq for CTC capture and gene expression profile analysis.[158] Hydro-Seq successfully sequenced the single cell RNA of 666 CTCs in 21 breast cancer patients. These CTCs were detected with ER\PR\AR and HER2 mutations, identifying the drug targets of hormone and targeted therapy for breast cancer, which can assist in the confirmation of targeted drug therapy. In addition, this study tracked individual cells expressing cancer stem cell (CSCs) and epithelial/mesenchymal cell state transition markers, which is beneficial to the study of tumor metastasis, treatment choice, and cell heterogeneity analysis. Kenji Kuroda *et al.* enriched CTCs by density gradient centrifugation and studied the blood samples of 100 patients with gastric cancer before gastrectomy.[159] Immunohistochemical evaluation showed that the number of FGFR2-positive CTCs in peripheral blood was significantly correlated with the expression of FGFR2 in primary gastric cancer. The relapse-free survival rate of FGFR2-positive CTCs

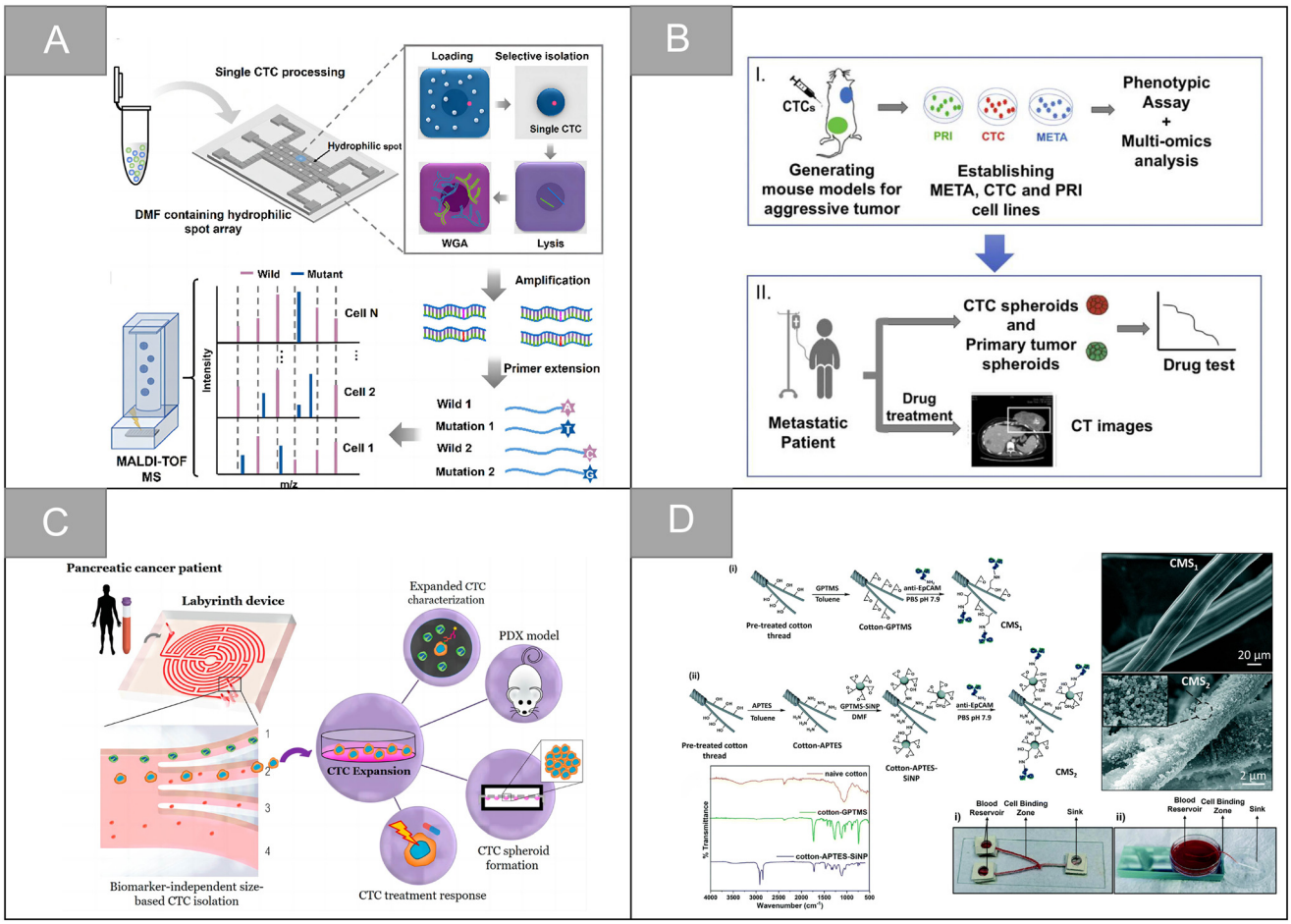

Fig. 11 Downstream analysis | (A) schematic illustration of DMF-scMS for the efficient and multiplex gene mutation profiling of single CTC[27] (reproduced with permission from ref. 27, Copyright 2022, American Chemical Society). (B) Schematic illustration of Multiomic characterization and drug testing[162] (reproduced with permission from ref. 162, Copyright 2022, Elsevier). (C) Schematic illustration of workflow for biomarker independent isolation, expansion, and analysis of CTCs[26] (reproduced with permission from ref. 26, Copyright 2020, MDPI). (D) Schematic representation of the synthesis of CMS[164] (reproduced with permission from ref. 164, Copyright 2022, Royal Society of Chemistry).

patients (≥5 cells/10 mL blood) was significantly lower than that of non-FGFR2-positive CTCs patients. Ruan *et al.* reported a single CTC mass spectrometry analysis platform DMF-scMS (Fig. 11A) based on digital microfluidic technology, which is used for single CTC isolation and multiple mutation analysis.[27] The KRAS mutation spectrum of heterogeneous CTCs at the single cell level in 5 patients with colorectal cancer was detected. At present, DMF-scMS is only suitable for the detection of known mutations in a single CTC. This is because it requires specific primers for single base extension of the mutation site and the known mUniz signal as a reference, but it still has great clinical potential in guiding accurate molecular targeted therapy for known mutation sites.

5.3 *Ex vivo* culture and testing of drug susceptibility

In vitro cultures from patients' tumor tissues can be used as an important alternative platform for evaluating different therapies, thus enabling clinicians to reliably predict individual patient responses. Compared with tumor tissue section culture, CTCs have a longer survival time and can be extracted from minimally invasive fluid biopsies in patients' peripheral blood, allowing regular samples to support real-time monitoring of clinical treatment efficacy and drug resistance development. In addition, CTC originated from the primary tumor, and the CTC line retained similar behavior and heterogeneous characteristics to cancer cells in the original tumor, with high uptake rate, rapid growth rate, similar tumor microenvironment and relatively low cost. The culture of CTCs *in vitro* not only provides a sufficient number of cells for other characterization, but also has great application potential in new drug screening and development, disease feature identification and biochemical mechanism research.

As shown in Fig. 11C, Lianette Rivera-Báez *et al.* used a size-based inertial microfluidic separation device to isolate CTC from the blood of 10 patients with advanced pancreatic cancer, and amplified it *in vitro* and characterized its function.[26] When tested with gemcitabine (gemcitabine) and 5FU (5-fluorouracil), CTC lines showed differences in drug sensitivity. Hu *et al.* used density gradient centrifugation and magnetic separation based on the CD45 antibody to separate HCC-CTC from patients' blood samples, and then used 3D culture to amplify the spheroids, and analyzed the relationship between clinicopathological variables of HCC patients and CTC spheres.[160] Lin *et al.* use the developed eSelect system to extract CTCs from blood samples of patients with head and neck cancer, then amplified them to form organ-like organs *in vitro*, and analyzed the drug sensitivity of cisplatin treatment, so as to predict the clinical drug response of patients with head and neck cancer.[161] Statistical analysis confirmed that the drug sensitivity of CTC-like organs *in vitro* was related to clinical response. The treatment accuracy of multivariate logical regression model for predicting chemotherapy response was 93.75%. The area under the curve (AUCs) of the prediction model was 0.8841 in the whole data set and 0.9167 in the cisplatin specific data set. As shown in Fig. 11B, Chen *et al.* separated CTCs based on a microfluidic chip modified by a biomimetic lipid membrane, established a CTC line *in vitro*, and carried out a multi-omics analysis and drug sensitivity test.[162] Phenotype, genome, epigenome and transcriptome analysis and drug test results of metastatic breast cancer patients show that the drug sensitivity of CTCs reflects the drug sensitivity of metastatic tumors, while the reaction of cells sampled from primary tumors is similar to that of primary tumors, indicating that CTCs and metastatic tumors are more similar. Ajay Balakrishnan *et al.* developed a short-term CTCs culture method in which cancer cell clusters were attached and proliferated by Matrigel coated in 96-well plates, and drug sensitivity tests were carried out in individual patients.[163] In the proof-of-concept experiment, CTCs were cultured from the blood of patients with baseline lung cancer and treated with the same drug regimen as patients with lung cancer. The survival rate of CTCs in the culture was 30.7%. The decrease in cell vitality was associated with the reduction of pleural effusion around the lungs of patients in actual treatment, showing the potential of this method in drug testing and personalized treatment. Smriti Arora *et al.* reported a cotton microfluidic substrate (CMS) that can effectively isolate CTCs and promote its expansion *in vitro* (Fig. 11D).[164] CMS with nanostructured surface can effectively isolate CTCs and act as a matrix to promote the formation of 3D tumor spheres in capturing cells, and its size increases by 5 times from the 3rd day to the 10th day of culture. In addition, when treated with the anticancer drug cisplatin, the tumor size was reduced by almost 1 to 2 within 24 hours. On the second and third day after cisplatin treatment, the tumor shrank and stopped, followed by the gradual growth of tumor globules, indicating that the tumor acquired drug resistance and demonstrated the potential of CMS in evaluating the efficacy of chemotherapy in drug discovery and development.

6 Conclusion and outlook

The application of CTC detection technology in clinical oncology has shown great promise in addressing numerous unmet needs. As current knowledge and understanding of cancer continue to evolve, cancer biologists and medical scientists hope to characterize the dynamic biology of the disease. This paper reviews various methodological methods of new early diagnosis techniques for cancer patients and various methods of separating and detecting CTC from whole blood. As mentioned above, these CTC strategies have significant advantages in non-invasive or minimally invasive diagnosis by liquid biopsy, improving the comfort of cancer patients by avoiding unnecessary and invasive tumor sampling.

Many kinds of CTC detection technologies have emerged, and dozens of different commercial CTC detection systems have been formed, such as CellSearch, CytoploRare, CTC-

Biopay, CellScan, and CellCollector. However, it is a pity that these methods are inadequate to some extent. Label-free enrichment based on physical characteristics can enrich many subtypes of CTC, but still have some problems. These include the easy blockage of the filter membrane or micropore, loss of small CTC, the need for pretreatment steps such as centrifugation and dilution, and lack of sufficient specificity of isolated cells. Enrichment based on biological characteristics has strong specificity, but it also has the limitation of being unable to capture heterogeneous CTCs. Due to the heterogeneity of tumors and the EMT process of tumors, the expression patterns of CTCs are different. However, at present, immune recognition is mainly limited to epithelial CTCs and the capture base on the expression of EpCAM. Although double antibodies and other recognition methods targeting multiple targets appear, other CTCs phenotypes will still be missed. The capture interface based on various nanostructures effectively enhances cells' capture and release ability, but the inherent limitations of immune recognition still limit it. In addition, CTC enrichment *in vitro* cannot avoid the problems of low flux and spatiotemporal heterogeneity of CTCs, and can only provide a few CTCs for downstream analysis. *In vivo* capture of CTC solves the problem of low flux to some extent, and a large number of CTCs can be obtained. However, heterogeneity still limits identification, and the detectable flux of CTC capture *in vivo* is still low for the human body.

The future direction of CTC enrichment is to solve these problems. As the ultimate goal of CTC enrichment is to maximize clinical application, obtaining reliable clinical data for future use and general acceptance by doctors, patients, and the government responsible for medical care is necessary to achieve standardization and repeatability of CTCs technology. Aiming to improve capture purity, capture capacity, flux, and the requirement of heterogeneous CTCs detection, module integration, and multi-mode detection is a possible direction based on existing enrichment technology of nanostructures. Module integration can combine the advantages of different enrichment methods to improve the enrichment effect. Multi-mode detection improves data reliability by mutual verification of different detection methods. *In vivo* CTC enrichment and collection/killing is another possible direction. *In vivo* enrichment has high throughput characteristics, and more CTC can be obtained. Negative enrichment is also a possible direction. This method can sort WBC and detect a variety of CTC subtypes. In addition, broad-spectrum enrichment of CTCs based on the metabolic characteristics of cancer cells (such as PH and lactic acid) and co-expressed biomolecules (such as FA and TA recognition) is a possible direction. However, more research is still needed in terms of capture purity and capture performance. Besides the development of CTC enrichment technology, the downstream analysis of CTCs is also essential to research content. The improvement of molecular analysis technology and the further study of the clinical value of CTCs will significantly promote the development of the CTC field, which requires the joint efforts of researchers in various related fields.

The concept of circulating tumor cells has been put forward for more than one hundred years. However, the capture and analysis of circulating tumor cells in the blood and their clinical application have been paid increasingly more attention in the past ten years. Previous studies have shown that CTC with tumor-related information can make up for traditional biopsy puncture difficulties and cannot monitor early cancer detection, judging patients' prognoses, predicting drug efficacy, and exploring the mechanism of drug resistance. However, to make full use of CTC in the clinic, it is still necessary to systematically understand the physiological mechanisms of CTC, improve the performance of the CTC enrichment platform and continue to study the clinical value of CTC. Today, with the emergence of ctDNA, exosomes, and a variety of new fluid biopsy markers, the value and future of CTC research is a question that all relevant researchers must face. The answer to this question can only rely on more in-depth research, which needs researchers in various related fields to continue to study the physiological mechanism of CTC, improve the CTC enrichment platform's performance and expand CTC's clinical application scenarios.

Author contributions

Lihua Guo: investigation, writing – revised draft. Chang Liu: investigation, writing – original draft. Manlin Qi: data curation, validation, formal analysis. Liang Cheng: conceptualization, project administration, writing – review & editing. Lin Wang: conceptualization, supervision, writing – review & editing, funding acquisition. Chunxia Li: conceptualization, supervision, writing – review & editing. Biao Dong: supervision, writing – review & editing.

Conflicts of interest

The authors declare no conflict of interest.

Acknowledgements

This work was supported by the National Natural Science Foundation of China (Grant No. 52250077, 52272080, 82073475), National Science Foundation of Jilin Province (20210401059YY, 20220402005GH, 20200801017GH), Major Basic Research Projects of Shandong Natural Science Foundation (ZR2020ZD36), Funding of Jilin Province Development and Reform Commission (2021C035-1), and the Natural Science Foundation of Jilin Province (20210401059YY, 20220402005GH).

References

1 T. Gansler, P. A. Ganz, M. Grant, F. L. Greene, P. Johnstone, M. Mahoney, L. A. Newman, W. K. Oh, C. R. Thomas Jr, M. J. Thun, A. J. Vickers, R. C. Wender and O. W. Brawley, *Ca-Cancer J. Clin.*, 2010, **60**, 345–350.

2 H. Sung, J. Ferlay, R. L. Siegel, M. Laversanne, I. Soerjomataram, A. Jemal and F. Bray, *Ca-Cancer J. Clin.*, 2021, **71**, 209–249.

3 S. de Wit, G. van Dalum and L. W. M. M. Terstappen, *Scientifica*, 2014, **2014**, 819362.
4 S. Paget, *Lancet*, 1889, **133**, 571–573.
5 K. Pantel and C. Alix-Panabières, *Trends Mol. Med.*, 2010, **16**, 398–406.
6 C. Alix-Panabières and K. Pantel, *Clin. Chem.*, 2013, **59**, 110–118.
7 S. Nagrath, L. V. Sequist, S. Maheswaran, D. W. Bell, D. Irimia, L. Ulkus, M. R. Smith, E. L. Kwak, S. Digumarthy and A. Muzikansky, *Nature*, 2007, **450**, 1235–1239.
8 J. S. De Bono, H. I. Scher, R. B. Montgomery, C. Parker, M. C. Miller, H. Tissing, G. V. Doyle, L. W. Terstappen, K. J. Pienta and D. Raghavan, *Clin. Cancer Res.*, 2008, **14**, 6302–6309.
9 E. Sollier, D. E. Go, J. Che, D. R. Gossett, S. O'Byrne, W. M. Weaver, N. Kummer, M. Rettig, J. Goldman and N. Nickols, *Lab Chip*, 2014, **14**, 63–77.
10 L. G. Martelotto, C. K. Ng, S. Piscuoglio, B. Weigelt and J. S. Reis-Filho, *Breast Cancer Res.*, 2014, **16**, 1–11.
11 A. A. Powell, A. H. Talasaz, H. Zhang, M. A. Coram, A. Reddy, G. Deng, M. L. Telli, R. H. Advani, R. W. Carlson and J. A. Mollick, *PLoS One*, 2012, **7**, e33788.
12 M. Labelle and R. O. Hynes, *Cancer Discovery*, 2012, **2**, 1091–1099.
13 C. V. Pecot, F. Z. Bischoff, J. A. Mayer, K. L. Wong, T. Pham, J. Bottsford-Miller, R. L. Stone, Y. G. Lin, P. Jaladurgam and J. W. Roh, *Cancer Discovery*, 2011, **1**, 580–586.
14 P. Paterlini-Brechot and N. L. Benali, *Cancer Lett.*, 2007, **253**, 180–204.
15 J. Chen, J. Li and Y. Sun, *Lab Chip*, 2012, **12**, 1753–1767.
16 Y.-F. Sun, X.-R. Yang, J. Zhou, S.-J. Qiu, J. Fan and Y. Xu, *J. Cancer Res. Clin. Oncol.*, 2011, **137**, 1151–1173.
17 M. C. Miller, G. V. Doyle and L. W. Terstappen, *J. Oncol.*, 2010, **2010**, 617421.
18 S. Riethdorf, H. Fritsche, V. Müller, T. Rau, C. Schindlbeck, B. Rack, W. Janni, C. Coith, K. Beck and F. Jänicke, *Clin. Cancer Res.*, 2007, **13**, 920–928.
19 A. H. Talasaz, A. A. Powell, D. E. Huber, J. G. Berbee, K.-H. Roh, W. Yu, W. Xiao, M. M. Davis, R. F. Pease and M. N. Mindrinos, *Proc. Natl. Acad. Sci. U. S. A.*, 2009, **106**, 3970–3975.
20 A. Li, X. He, J. Wu, J. Zhang, G. Xu, B. Xu, G. Zhao and Z. Shen, *Lab Chip*, 2022, **22**, 3676–3686.
21 C. Li, S. Yang, R. Li, S. Gong, M. Huang, Y. Sun, G. Xiong, D. Wu, M. Ji and Y. Chen, *ACS Appl. Mater. Interfaces*, 2022, **14**, 7646–7658.
22 H. Cui, Q. Liu, R. Li, X. Wei, Y. Sun, Z. Wang, L. Zhang, X.-Z. Zhao, B. Hua and S.-S. Guo, *Nanoscale*, 2020, **12**, 1455–1463.
23 Y. Hu, W. Tang, P. Cheng, Q. Zhou, X. Tian, X. Wei and H. He, *Cytometry, Part A*, 2019, **95**, 657–663.
24 P. Hai, Y. Qu, Y. Li, L. Zhu, L. Shmuylovich, L. A. Cornelius and L. V. Wang, *J. Biomed. Opt.*, 2020, **25**, 036002.
25 T. H. Kim, Y. Wang, C. R. Oliver, D. H. Thamm, L. Cooling, C. Paoletti, K. J. Smith, S. Nagrath and D. F. Hayes, *Nat. Commun.*, 2019, **10**, 1–8.
26 L. Rivera-Báez, I. Lohse, E. Lin, S. Raghavan, S. Owen, R. Harouaka, K. Herman, G. Mehta, T. S. Lawrence and M. A. Morgan, *Cancers*, 2020, **12**, 1011.
27 Q. Ruan, J. Yang, F. Zou, X. Chen, Q. Zhang, K. Zhao, X. Lin, X. Zeng, X. Yu and L. Wu, *Anal. Chem.*, 2021, **94**, 1108–1117.
28 C. Li, R. Li, X. Wu, Y. Zuo, G. Xiong, M. Huang, Y. Sun, R. Liao, Y. Xiao and L. Hu, *Anal. Chem.*, 2022, **94**, 15240–15249.
29 H. M. Shapiro, E. R. Schildkraut, R. Curbelo, C. W. Laird, B. Turner and T. Hirschfeld, *J. Histochem. Cytochem.*, 1976, **24**, 396–401.
30 P. Bankó, S. Y. Lee, V. Nagygyörgy, M. Zrínyi, C. H. Chae, D. H. Cho and A. Telekes, *J. Hematol. Oncol.*, 2019, **12**, 1–20.
31 X. Xu, Z. Jiang, J. Wang, Y. Ren and A. Wu, *Electrophoresis*, 2020, **41**, 933–951.
32 M. Hosokawa, T. Hayata, Y. Fukuda, A. Arakaki, T. Yoshino, T. Tanaka and T. Matsunaga, *Anal. Chem.*, 2010, **82**, 6629–6635.
33 S. Zheng, H. Lin, J.-Q. Liu, M. Balic, R. Datar, R. J. Cote and Y.-C. Tai, *J. Chromatogr. A*, 2007, **1162**, 154–161.
34 X. Xu, J. Lin, Y. Guo, X. Wu, Y. Xu, D. Zhang, X. Zhang, X. Yujiao, J. Wang and C. Yao, *Biosens. Bioelectron.*, 2022, **210**, 114305.
35 A. F. Sarioglu, N. Aceto, N. Kojic, M. C. Donaldson, M. Zeinali, B. Hamza, A. Engstrom, H. Zhu, T. K. Sundaresan and D. T. Miyamoto, *Nat. Methods*, 2015, **12**, 685–691.
36 M. Boya, T. Ozkaya-Ahmadov, B. E. Swain, C.-H. Chu, N. Asmare, O. Civelekoglu, R. Liu, D. Lee, S. Tobia and S. Biliya, *Nat. Commun.*, 2022, **13**, 1–13.
37 A. Lee, J. Park, M. Lim, V. Sunkara, S. Y. Kim, G. H. Kim, M.-H. Kim and Y.-K. Cho, *Anal. Chem.*, 2014, **86**, 11349–11356.
38 Q. Huang, F.-B. Wang, C.-H. Yuan, Z. He, L. Rao, B. Cai, B. Chen, S. Jiang, Z. Li and J. Chen, *Theranostics*, 2018, **8**, 1624.
39 H. J. Woo, S.-H. Kim, H. J. Kang, S.-H. Lee, S. J. Lee, J. M. Kim, O. Gurel, S. Y. Kim, H. R. Roh and J. Lee, *Theranostics*, 2022, **12**, 3676.
40 I.-F. Cheng, W.-L. Huang, T.-Y. Chen, C.-W. Liu, Y.-D. Lin and W.-C. Su, *Lab Chip*, 2015, **15**, 2950–2959.
41 T. Luo, L. Fan, Y. Zeng, Y. Liu, S. Chen, Q. Tan, R. H. Lam and D. Sun, *Lab Chip*, 2018, **18**, 1521–1532.
42 P. Modarres and M. Tabrizian, *Sens. Actuators, B*, 2019, **286**, 493–500.
43 J. Park, C. Park, Y. Sugitani, T. Fujii and S. H. Kim, *Lab Chip*, 2022, **22**, 3000–3007.
44 P. Augustsson, C. Magnusson, M. Nordin, H. Lilja and T. Laurell, *Anal. Chem.*, 2012, **84**, 7954–7962.
45 M. Antfolk, C. Magnusson, P. Augustsson, H. Lilja and T. Laurell, *Anal. Chem.*, 2015, **87**, 9322–9328.
46 S. Karthick, P. N. Pradeep, P. Kanchana and A. K. Sen, *Lab Chip*, 2018, **18**, 3802–3813.
47 E. Undvall Anand, C. Magnusson, A. Lenshof, Y. Ceder, H. Lilja and T. Laurell, *Anal. Chem.*, 2021, **93**, 17076–17085.

48 S. C. Hur, H. T. K. Tse and D. Di Carlo, *Lab Chip*, 2010, **10**, 274–280.
49 A. J. Mach and D. Di Carlo, *Biotechnol. Bioeng.*, 2010, **107**, 302–311.
50 M. E. Warkiani, B. L. Khoo, L. Wu, A. K. P. Tay, A. A. S. Bhagat, J. Han and C. T. Lim, *Nat. Protoc.*, 2016, **11**, 134–148.
51 F. Tian, L. Cai, J. Chang, S. Li, C. Liu, T. Li and J. Sun, *Lab Chip*, 2018, **18**, 3436–3445.
52 R. Guglielmi, Z. Lai, K. Raba, G. van Dalum, J. Wu, B. Behrens, A. A. S. Bhagat, W. T. Knoefel, R. P. L. Neves and N. H. Stoecklein, *Sci. Rep.*, 2020, **10**, 1–9.
53 Y. Fang, S. Zhu, W. Cheng, Z. Ni and N. Xiang, *Lab Chip*, 2022, **22**, 3545–3554.
54 N. Xiang, J. Wang, Q. Li, Y. Han, D. Huang and Z. Ni, *Anal. Chem.*, 2019, **91**, 10328–10334.
55 Y. Wu, R. Chattaraj, Y. Ren, H. Jiang and D. Lee, *Anal. Chem.*, 2021, **93**, 7635–7646.
56 C.-Y. Wen, L.-L. Wu, Z.-L. Zhang, Y.-L. Liu, S.-Z. Wei, J. Hu, M. Tang, E.-Z. Sun, Y.-P. Gong and J. Yu, *ACS Nano*, 2014, **8**, 941–949.
57 Z. Wang, N. Sun, H. Liu, C. Chen, P. Ding, X. Yue, H. Zou, C. Xing and R. Pei, *ACS Appl. Mater. Interfaces*, 2019, **11**, 39586–39593.
58 M. Hu, C. Li, Z. Wang, P. Ding, R. Pei, Q. Wang, H. Xu and C. Xing, *Front. Bioeng. Biotechnol.*, 2022, 90.
59 W. Xia, H. Li, Y. Li, M. Li, J. Fan, W. Sun, N. Li, R. Li, K. Shao and X. Peng, *Nano Lett.*, 2020, **21**, 634–641.
60 Z. Liao, L. Han, Q. Li, L. Li, Y. Liu, Y. Song, W. Tan and E. Song, *Adv. Funct. Mater.*, 2021, **31**, 2009937.
61 L.-L. Wu, C.-Y. Wen, J. Hu, M. Tang, C.-B. Qi, N. Li, C. Liu, L. Chen, D.-W. Pang and Z.-L. Zhang, *Biosens. Bioelectron.*, 2017, **94**, 219–226.
62 L.-L. Wu, Z.-L. Zhang, M. Tang, D.-L. Zhu, X.-J. Dong, J. Hu, C.-B. Qi, H.-W. Tang and D.-W. Pang, *Angew. Chem., Int. Ed.*, 2020, **59**, 11240–11244.
63 H. Guo, X. Song, W. Lei, C. He, W. You, Q. Lin, S. Zhou, X. Chen and Z. Chen, *Angew. Chem., Int. Ed.*, 2019, **58**, 12195–12199.
64 J. Lyu, H. Xu, B. Dong, C. Li, S. Yu, S. Hu, B. Zhou, L. Wang and H. Song, *Chem. Eng. J.*, 2022, **448**, 137761.
65 X. Liu, F. Wang, Y. Meng, L. Zhao, W. Shi, X. Wang, Z. He, J. Chao and C. Li, *Biosens. Bioelectron.*, 2022, **207**, 114208.
66 L. Rao, Q.-F. Meng, Q. Huang, Z. Wang, G.-T. Yu, A. Li, W. Ma, N. Zhang, S.-S. Guo and X.-Z. Zhao, *Adv. Funct. Mater.*, 2018, **28**, 1803531.
67 X. Wu, Z. Lin, C. Zhao, L. Liu, K. Zhang, J. Lai, Q.-F. Meng, G. Yao, Q. Huang and X.-Z. Zhao, *Biosens. Bioelectron.*, 2022, 114425.
68 S. Fang, C. Wang, J. Xiang, L. Cheng, X. Song, L. Xu, R. Peng and Z. Liu, *Nano Res.*, 2014, **7**, 1327–1336.
69 Z. Li, G. Wang, Y. Shen, N. Guo and N. Ma, *Adv. Funct. Mater.*, 2018, **28**, 1707152.
70 Y. Wang, T. Huo, Y. Du, M. Qian, C. Lin, H. Nie, W. Li, T. Hao, X. Zhang and N. Lin, *Biosens. Bioelectron.*, 2022, **215**, 114530.
71 C. Ding, C. Zhang, X. Yin, X. Cao, M. Cai and Y. Xian, *Anal. Chem.*, 2018, **90**, 6702–6709.
72 C. Ding, C. Zhang, S. Cheng and Y. Xian, *Adv. Funct. Mater.*, 2020, **30**, 1909781.
73 P. Chen, Y. Wang, Y. He, K. Huang, X. Wang, R. Zhou, T. Liu, R. Qu, J. Zhou and W. Peng, *ACS Nano*, 2021, **15**, 11634–11643.
74 Y. Peng, B. Lu, Y. Deng, N. Yang and G. Li, *Biosens. Bioelectron.*, 2022, **201**, 113973.
75 M. Li, J. Liu, X. Wang, J. Wang, L.-H. Huang, M. Gao and X. Zhang, *Anal. Chem.*, 2022, **94**, 15076–15084.
76 D.-X. Wang, J. Wang, Y.-X. Wang, J.-Y. Ma, B. Liu, A.-N. Tang and D.-M. Kong, *Chem. Sci.*, 2022, **13**, 10395–10405.
77 N.-N. Lu, M. Xie, J. Wang, S.-W. Lv, J.-S. Yi, W.-G. Dong and W.-H. Huang, *ACS Appl. Mater. Interfaces*, 2015, **7**, 8817–8826.
78 L. Bai, Y. Du, J. Peng, Y. Liu, Y. Wang, Y. Yang and C. Wang, *J. Mater. Chem. B*, 2014, **2**, 4080–4088.
79 J. Peng, Q. Zhao, W. Zheng, W. Li, P. Li, L. Zhu, X. Liu, B. Shao, H. Li and C. Wang, *ACS Appl. Mater. Interfaces*, 2017, **9**, 18423–18428.
80 F. Jia, Y. Wang, Z. Fang, J. Dong, F. Shi, W. Zhang, Z. Wang and Z. Hu, *Anal. Chem.*, 2021, **93**, 5670–5675.
81 R. Han, Y. Li, M. Chen, W. Li, C. Ding and X. Luo, *Anal. Chem.*, 2022, **94**, 2204–2211.
82 T. Li, N. Li, Y. Ma, Y.-J. Bai, C.-M. Xing and Y.-K. Gong, *J. Mater. Chem. B*, 2019, **7**, 6087–6098.
83 J. Bu, W. Jeong, R. Jafari, L. J. Kubiatowicz, A. Nair, M. J. Poellmann, R. S. Hong, E. W. Liu, R. H. Owen and P. A. Rawding, *Biosens. Bioelectron.*, 2022, 114445.
84 L. Du, W. Chen, J. Wang, W. Cai, S. Kong and C. Wu, *Sens. Actuators, B*, 2019, **301**, 127073.
85 Y. Hu, D. Chen, J. V. Napoleon, M. Srinivasarao, S. Singhal, C. A. Savran and P. S. Low, *Sci. Rep.*, 2022, **12**, 1–10.
86 T. Zhang, W. Peng, W. Jiang, K. Gao and W. Liu, *ACS Appl. Mater. Interfaces*, 2021, **13**, 24543–24552.
87 P. Chen, Y. He, T. Liu, F. Li, K. Huang, D. Tang, P. Jiang, S. Wang, J. Zhou and J. Huang, *Biosens. Bioelectron.*, 2022, **202**, 114009.
88 Y. Xu, J. Lin, X. Wu, X. Xu, D. Zhang, Y. Xie, T. Pan, Y. He, A. Wu and G. Shao, *J. Mater. Chem. B*, 2022, **10**, 3808–3816.
89 S. Sun, R. Wang, Y. Huang, J. Xu, K. Yao, W. Liu, Y. Cao and K. Qian, *Small*, 2019, **15**, 1902441.
90 Y. Zhang, W. Wang, H. Guo, M. Liu, H. Zhu and H. Sun, *Nanotechnology*, 2021, **32**, 475102.
91 X. Li, T. Cui, W. Zhang, Z. Zhai, F. Wu, Y. Zhang, M. Yang, W. Zhong and W. Yue, *Colloids Surf., B*, 2020, **196**, 111281.
92 D. Yin, A. Shi, B. Zhou, M. Wang, G. Xu, M. Shen, X. Zhu and X. Shi, *Langmuir*, 2022, **38**, 11080–11086.
93 M. Schmidt, A. Franken, D. Wilms, T. Fehm, H. J. Neubauer and S. Schmidt, *ACS Appl. Bio Mater.*, 2021, **4**, 6371–6380.
94 L. Yang, H. Sun, W. Jiang, T. Xu, B. Song, R. Peng, L. Han and L. Jia, *Chem. Mater.*, 2018, **30**, 4372–4382.
95 P. Ding, Z. Wang, Z. Wu, M. Hu, W. Zhu, N. Sun and R. Pei, *ACS Appl. Mater. Interfaces*, 2021, **13**, 3694–3700.

96 Y. Zhou, X. Wang, Z. Luo, X. Liu, J. Hou and S. Zhou, *Small Sci.*, 2022, **2**, 2200061.
97 F. Zhang, Y. Jiang, X. Liu, J. Meng, P. Zhang, H. Liu, G. Yang, G. Li, L. Jiang and L.-J. Wan, *Nano Lett.*, 2016, **16**, 766–772.
98 H. Xu, B. Dong, S. Xu, S. Xu, X. Sun, J. Sun, Y. Yang, L. Xu, X. Bai and S. Zhang, *Biomaterials*, 2017, **138**, 69–79.
99 S. Li, K. Wang, S. Hao, F. Dang, Z.-Q. Zhang and J. Zhang, *Anal. Chem.*, 2022, **94**, 6754–6759.
100 J. Li, Y. Yuan, H. Gan, C. Dong, B. Cao, J. Ni, X. Li, W. Gu, C. Song and L. Wang, *ACS Appl. Mater. Interfaces*, 2022, **14**, 32869–32879.
101 V. Shirmohammadli, N. Manavizadeh and Z. G. Bafghi, *IEEE Sens. J.*, 2019, **20**, 591–598.
102 H. Su, S. Yin, J. Yang, Y. Wu, C. Shi, H. Sun and G. Wang, *Electrochim. Acta*, 2021, **393**, 139093.
103 J. Xu, C. Zhao, K. Niu, Z. Gao and Y.-Y. Song, *Anal. Chim. Acta*, 2021, **1142**, 1–9.
104 W. Li, R. Li, B. Huang, Z. Wang, Y. Sun, X. Wei, C. Heng, W. Liu, M. Yu and S.-S. Guo, *Nanotechnology*, 2019, **30**, 335101.
105 J. Fan, Z. Dang, T. Lu, J. Li, T. Chen, Y. Yang and X. Li, *J. Mater. Sci.*, 2021, **56**, 16634–16647.
106 N. Sun, M. Liu, J. Wang, Z. Wang, X. Li, B. Jiang and R. Pei, *Small*, 2016, **12**, 5090–5097.
107 C. Chen, Z. Wu, P. Ding, N. Sun, H. Liu, Y. Chen, Z. Wang and R. Pei, *Adv. Fiber Mater.*, 2020, **2**, 186–193.
108 Z. Wu, Y. Pan, Z. Wang, P. Ding, T. Gao, Q. Li, M. Hu, W. Zhu and R. Pei, *J. Mater. Chem. B*, 2021, **9**, 2212–2220.
109 Y. Zhao, J. Xiong, X. Shi and F. Ko, *Colloids Surf., A*, 2019, **583**, 123978.
110 Y. Zhu, C. Zou, J. Zhang, W. Jiang, F. Guan, K. Tang, S. Li, G. Li, J. Wang and Z. Ke, *ACS Appl. Mater. Interfaces*, 2020, **12**, 5671–5679.
111 H. Zhong, C. Yuan, J. He, Y. Yu, Y. Jin, Y. Huang and R. Zhao, *Anal. Chem.*, 2021, **93**, 9778–9787.
112 M. Wang, Y. Tan, D. Li, G. Xu, D. Yin, Y. Xiao, T. Xu, X. Chen, X. Zhu and X. Shi, *Adv. Fiber Mater.*, 2021, **3**, 192–202.
113 R. Khan, A. Radoi, S. Rashid, A. Hayat, A. Vasilescu and S. Andreescu, *Sensors*, 2021, **21**, 3369.
114 H. J. Yoon, T. H. Kim, Z. Zhang, E. Azizi, T. M. Pham, C. Paoletti, J. Lin, N. Ramnath, M. S. Wicha and D. F. Hayes, *Nat. Nanotechnol.*, 2013, **8**, 735–741.
115 B. Dou, L. Xu, B. Jiang, R. Yuan and Y. Xiang, *Anal. Chem.*, 2019, **91**, 10792–10799.
116 X. Zhou, Y. Zhang, K. Kang, N. Zhu, J. Cheng, Q. Yi and Y. Wu, *J. Mater. Chem. B*, 2022, **10**, 3119–3125.
117 Q. You, J. Peng, Z. Chang, M. Ge, Q. Mei and W.-F. Dong, *Talanta*, 2021, **235**, 122770.
118 C. Shen, L. Zhong, L. Xiong, C. Liu, L. Yu, X. Chu, X. Luo, M. Zhao and B. Liu, *Sens. Actuators, B*, 2021, **331**, 129399.
119 S. Wang, J. Cui, Q. Fan, J. Gan, C. Liu, Y. Wang, T. Yang, J. Wang and C. Yang, *Anal. Chem.*, 2022, **94**, 9450–9458.
120 W. Wang, G. Yang, H. Cui, J. Meng, S. Wang and L. Jiang, *Adv. Healthcare Mater.*, 2017, **6**, 1700003.
121 Y. Chen, D. Tyagi, M. Lyu, A. J. Carrier, C. Nganou, B. Youden, W. Wang, S. Cui, M. Servos and K. Oakes, *Anal. Chem.*, 2019, **91**, 4017–4022.
122 L. Jia, X. Zhen, L. Chen, Q. Feng, W. Yuan, Y. Bu, S. Wang and X. Xie, *J. Colloid Interface Sci.*, 2023, **631**, 55–65.
123 X. Zhang, X. Wei, X. Men, C.-X. Wu, J.-J. Bai, W.-T. Li, T. Yang, M.-L. Chen and J.-H. Wang, *ACS Appl. Mater. Interfaces*, 2021, **13**, 43668–43675.
124 X. Dou, P. Li, S. Jiang, H. Bayat and H. Schönherr, *ACS Appl. Mater. Interfaces*, 2017, **9**, 8508–8518.
125 L. Wang, S. Huang, Q.-Y. Li, L.-Y. Ma, C. Zhang, F. Liu, M. Jiang, X. Yu and L. Xu, *Chem. Eng. J.*, 2022, **435**, 134762.
126 M. G. Ahmed, M. F. Abate, Y. Song, Z. Zhu, F. Yan, Y. Xu, X. Wang, Q. Li and C. Yang, *Angew. Chem., Int. Ed.*, 2017, **56**, 10681–10685.
127 H. Shen, R. Su, J. Peng, L. Zhu, K. Deng, Q. Niu, Y. Song, L. Yang, L. Wu and Z. Zhu, *Bioact. Mater.*, 2022, **11**, 32–40.
128 M. Rahmanian, O. S. Hematabad, E. Askari, F. Shokati, A. Bakhshi, S. Moghadam, A. Olfatbakhsh, E. A. S. Hashemi, M. K. Ahmadi and S. M. Naghib, *J. Adv. Res.*, 2022, **08**, 005.
129 B. J. Green, M. Marazzini, B. Hershey, A. Fardin, Q. Li, Z. Wang, G. Giangreco, F. Pisati, S. Marchesi and A. Disanza, *Small*, 2022, **18**, 2106097.
130 A. Abdulla, Z. Zhang, K. Z. Ahmad, A. R. Warden, H. Li and X. Ding, *Biosens. Bioelectron.*, 2022, **201**, 113965.
131 X. Chen, H. Ding, D. Zhang, K. Zhao, J. Gao, B. Lin, C. Huang, Y. Song, G. Zhao and Y. Ma, *Adv. Sci.*, 2021, **8**, 2102070.
132 E. A. Kwizera, W. Ou, S. Lee, S. Stewart, J. G. Shamul, J. Xu, N. Tait, K. H. Tkaczuk and X. He, *ACS Nano*, 2022, **16**, 11374–11391.
133 K. Pang, B. Gu, F. Liu, M. Dong, L. Zhu and X. Wei, *J. Innovative Opt. Health Sci.*, 2019, **12**, 1930008.
134 J. Novak, I. Georgakoudi, X. Wei, A. Prossin and C. P. Lin, *Opt. Lett.*, 2004, **29**, 77–79.
135 H. Lee, C. Alt, C. M. Pitsillides, M. Puoris'haag and C. P. Lin, *Opt. Express*, 2006, **14**, 7789–7800.
136 W. He, H. Wang, L. C. Hartmann, J.-X. Cheng and P. S. Low, *Proc. Natl. Acad. Sci. U. S. A.*, 2007, **104**, 11760–11765.
137 H. Seo, Y. Hwang, K. Choe and P. Kim, *Biomed. Opt. Express*, 2015, **6**, 2158–2167.
138 R. A. Patil, M. Srinivasarao, M. M. Amiji, P. S. Low and M. Niedre, *Mol. Imaging Biol.*, 2020, **22**, 1280–1289.
139 N. Ding, Monitoring circulating tumor cells in prostate cancer model after tumor resection by in vivo flow cytometry, *MPhil*, Shanghai Jiao Tong University, 2019.
140 Y. Zhou, Developing in vivo photoacoustic flow cytometry technique for detection of circulating melanoma cells, *MPhil*, Shanghai Jiao Tong University, 2019.
141 C. Li and L. V. Wang, *Phys. Med. Biol.*, 2009, **54**, R59.
142 A. Karabutov, N. B. Podymova and V. S. Letokhov, *Appl. Phys. B: Lasers Opt.*, 1996, **63**, 545–563.
143 P. Yang, D. Wei, K. Pang, Q.-Y. Wang, Q.-Y. Zhou and X.-B. Wei, *Laser Optoelectron. Prog.*, 2017, **54**, 090001.
144 J. Weber, P. C. Beard and S. E. Bohndiek, *Nat. Methods*, 2016, **13**, 639–650.

145 C. Jia, S.-W. Huang, Y. Jin, C. H. Seo, L. Huang, J. F. Eary, X. Gao and M. O'Donnell, in *Photons Plus Ultrasound: Imaging and Sensing 2010*, SPIE, 2010, vol. 7564, pp. 275–280.
146 Y. Jin, C. Jia, S.-W. Huang, M. O'donnell and X. Gao, *Nat. Commun.*, 2010, **1**, 1–8.
147 M. Mehrmohammadi, J. Oh, S. Mallidi and S. Y. Emelianov, *Mol. Imaging*, 2011, **10**, 7290.2010.00037.
148 X. Hu, C.-W. Wei, J. Xia, I. Pelivanov, M. O'Donnell and X. Gao, *Small*, 2013, **9**, 2046.
149 O. Vermesh, A. Aalipour, T. J. Ge, Y. Saenz, Y. Guo, I. S. Alam, S. Park, C. N. Adelson, Y. Mitsutake and J. Vilches-Moure, *Nat. Biomed. Eng.*, 2018, **2**, 696–705.
150 S.-B. Cheng, M. Wang, C. Zhang, M.-M. Chen, Y.-K. Wang, S. Tian, N. Zhan, W.-G. Dong, M. Xie and W.-H. Huang, *Anal. Chem.*, 2020, **92**, 5447–5455.
151 D. Wang, R. Dong, X. Wang and X. Jiang, *ACS Nano*, 2022, **16**, 5274–5283.
152 Z. Yin, R. Shi, X. Xia, L. Li, Y. Yang, S. Li, J. Xu, Y. Xu, X. Cai and S. Wang, *Adv. Mater.*, 2022, 2207870.
153 H. Zhang, Z. Jia, C. Wu, L. Zang, G. Yang, Z. Chen and B. Tang, *ACS Appl. Mater. Interfaces*, 2015, **7**, 20477–20484.
154 J. Li, X. Li, Y. Zhang, K. Jin, Y. Yuan, R. Ming, Y. Yang and T. Chen, *Nano Res.*, 2022, 1–9.
155 D. Wang, C. Ge, W. Liang, Q. Yang, Q. Liu, W. Ma, L. Shi, H. Wu, Y. Zhang and Z. Wu, *Adv. Sci.*, 2020, **7**, 2000940.
156 S. Wan, T. H. Kim, K. J. Smith, R. Delaney, G.-S. Park, H. Guo, E. Lin, T. Plegue, N. Kuo and J. Steffes, *Sci. Rep.*, 2019, **9**, 1–11.
157 X.-H. Ren, X.-Y. He, C. Xu, D. Han and S.-X. Cheng, *Adv. Sci.*, 2022, 2105806.
158 Y.-H. Cheng, Y.-C. Chen, E. Lin, R. Brien, S. Jung, Y.-T. Chen, W. Lee, Z. Hao, S. Sahoo and H. M. Kang, *Nat. Commun.*, 2019, **10**, 1–11.
159 K. Kuroda, M. Yashiro, Y. Miki, T. Sera, Y. Yamamoto, A. Sugimoto, S. Nishimura, S. Kushiyama, S. Togano and T. Okuno, *Cancer Sci.*, 2020, **111**, 4500–4509.
160 C.-L. Hu, Y.-J. Zhang, X.-F. Zhang, X. Fei, H. Zhang, C.-G. Li and B. Sun, *OncoTargets Ther.*, 2021, **14**, 2673.
161 K.-C. Lin, L.-L. Ting, C.-L. Chang, L.-S. Lu, H.-L. Lee, F.-C. Hsu, J.-F. Chiou, P.-Y. Wang, T. Burnouf, D. C.-Y. Ho, K.-C. Yang, C.-Y. Chen, C.-H. Chen, C.-Z. Wu and Y.-J. Chen, *Cancers*, 2021, **13**, 6076.
162 J.-Y. Chen, H.-H. Chou, S. C. Lim, Y.-J. Huang, K.-C. Lai, C.-L. Guo, C.-Y. Tung, C.-T. Su, J. Wang and E. Liu, *iScience*, 2022, **25**, 105081.
163 A. Balakrishnan, A. G. F. Thottian, K. Govind Babu and P. Kumar, *Med. Oncol.*, 2023, **40**, 1–6.
164 S. Arora, A. D'Souza, G. Aland, N. Kale, B. Jadhav, T. Kad, P. Chaturvedi, B. Singh and J. Khandare, *Lab Chip*, 2022, **22**, 1519–1530.